Received: 26 July 2024 | Revised: 10 November 2024 | Accepted: 7 December 2024

IET Communications

DOI: 10.1049/cmu2.12873

The Institution of Engineering and Technology WILEY

ORIGINAL RESEARCH

# MMSE-based passive beamforming for reconfigurable intelligent surface aided millimeter wave MIMO

**Prabhat Raj Gautam**[1] | **Li Zhang**[1] | **Pingzhi Fan**[2]

[1]School of Electronic and Electrical Engineering, University of Leeds, Leeds, UK

[2]Institute of Mobile Communications, Southwest Jiaotong University, Chengdu, China

**Correspondence**
Li Zhang, School of Electronic and Electrical Engineering, University of Leeds, Leeds, UK.
Email: l.x.zhang@leeds.ac.uk

**Abstract**

Reconfigurable intelligent surfaces (RISs) have emerged as propitious solution to configure random wireless channel into suitable propagation environment by adjusting a large number of low-cost passive reflecting elements. It is considered that narrowband downlink millimeter wave (mmWave) multiple-input multiple-output (MIMO) communication is aided by deploying an RIS. Large antenna arrays are used to counter the huge propagation loss suffered by the mmWave signals. Hybrid precoding in which precoding is performed in digital and analog domains is employed to reduce the number of costly and power-consuming radio frequency (RF) chains. Passive beamforming at RIS is designed together with precoder and combiner through joint optimization problem to minimize the mean square error between the transmit signal and the estimate of signal at the receiver. The optimization problem is solved by an iterative procedure in which solution to the non-convex reflecting coefficients design problem is approximated by extracting the phases of the solution to unconstrained problem without unit amplitude constraint of the reflecting elements. It is shown that the proposed design principle also applies to the wideband channel. Simulation results show that the proposed design delivers performance better than existing state-of-the-art solutions, but at lower complexity.

## 1 | INTRODUCTION

Millimeter wave (mmWave) communication offers large pristine bandwidth that provides the future wireless communication technology a key to unleash the potential of achieving very high data rates in order of tens of gigabits-dper-second [1–5]. The small wavelengths of mmWave signals make them vulnerable to huge path loss [6, 7]. However, we can employ massive multiple-input multiple-output (MIMO) to harvest large array gain and reimburse the loss. It is challenging to have a reliable communication in mmWave as shadowing affects the average received power so severely [8] that no link existing between the transmitter and the user can be a common phenomenon, especially in the dense urban areas [9]. In such low-received power scenarios, the reconfigurable intelligent surface (RIS) can function as centralized beamformer to increase channel gains [8]. RIS can create virtual line of sight (LoS) path between the base station (BS) and the receiver to elude the impeding objects between the BS and the receiver [8, 10] by re-radiating signal in the shape of a beam toward the receiver [11].

An RIS is a metasurface consisting of a number of elements capable of reflecting the incident signal without the need for RF processing, decoding, encoding, or retransmission [10, 12, 13]. Controlling the way electromagnetic wave behaves by introducing changes in the phases only (nearly-passive RIS) or amplitudes and phases (active RIS) of the incident signals, RIS can engender a programmable, highly deterministic radio environments from highly probabilistic wireless environment [14–17]. Such radio channel makes the transfer and processing of information between transmitters and receivers more reliable [15, 18]. Most of the RISs considered in the literature are capable of introducing only the phase changes to the impinging waves. The RISs have been envisaged to be operated by evaluating the phase shift coefficients at the BS based on the channel state information (CSI), and controlling the RIS through a smart controller such as a field programmable gate array (FPGA) [19]. The

proper design of phase response of RIS can achieve useful signal enhancement and/or interference suppression to produce high-quality passive beamforming [20]. Thus, design of phase shift coefficients of RIS is also called passive beamforming design.

Ning et al. [21] consider an RIS-aided point-to-point MIMO, and propose to design passive beamforming by sum-path-gain maximization (SPGM) with the view to maximize the sum of gains of different channel paths, or effectively the channel power. The SPGM problem is solved by alternating direction of method of multipliers (ADMM), and singular value decomposition (SVD) is performed on the equivalent channel subsequently to construct transmit precoder. Wang et al. [22] seek to jointly optimize the transmitter precoding vector and RIS phase-shifts by maximizing the received signal power in an mmWave MIMO environment assisted by multiple RISs. An optimal closed-form solution is obtained for single RIS case, whereas near-optimal analytical solution is derived for multi-RIS case by assuming near-orthogonality of different steering vectors. In [23], authors jointly design the precoder at the access point (AP) and the phases of the RIS elements to maximize the weighted sum-rate in an RIS-aided multiple user multiple-input single-output (MU-MISO) downlink system by designing a solution based on fractional programming. Pan et al. [19] and Zhang et al. [24] also aim to maximize weighted sum-rate of all users through joint optimization. The authors in [19] consider a multi-cell MIMO with multi-antenna users, while [24] considers cell free MIMO with multi-antenna users and multiple RISs. The problem is solved by alternating optimization in both [19] and [24]. Fractional programming is used in [24] to split the problem into multiple subproblems which are solved alternately. Reference [19] optimizes the phase-shifts of RIS through majorization-minimization algorithm and complex circle manifold method. Zhao et al. [25] jointly optimize the precoding at the AP and discrete phase shifts of the RIS with the aim of minimizing AP's transmit power constrained to the outage probability for the users. Liu et al. [26] decouple the joint symbol-level precoding and reflection coefficients design problem in MU-MISO systems, and solves the symbol-level precoding and the reflection coefficients design subproblems by using algorithms based on gradient-projection and Riemannian conjugate gradient, respectively. Zhang et al. [27] and Wang et al. [9] both consider joint optimization of active and passive beamforming in point-to-point MIMO aided by a single RIS. Reference [27] alternately optimizes the transmit covariance matrix and the phase-shift coefficients of the RIS. Reference [9] exploits the structure of mmWave channel and reconstructs the complex joint optimization problem into a simpler problem which is solved by a manifold optimization algorithm. The authors adopt manifold based optimization method [28] to generate hybrid precoder. Similarly, Hong et al. [29] and Wang et al. [30] also adopt joint design of hybrid precoder at the transmitter and passive beamforming at the RIS. By exploiting sparse-scattering structure and large dimension of mmWave channels, [29] proposes the method of RIS design which is based on asymptotically maximizing the eigenvalue associated with the dominant transmit–receive path pair at the RIS. In [30], the structure of effective mmWave channel is leveraged to simplify joint optimization of transmit precoding and passive beamforming to develop passive beamforming method based on manipulating the singular values of the effective channel. The passive beamforming proposed in [30], in fact, extends the method proposed in [9] by also considering the direct channel between the transmitter and the receiver. Moreover, the passive beamforming in [30] is designed to operate in wideband MIMO-OFDM channel, unlike [9] which only works in narrowband channel. Ning et al. [31] model RIS phase shift design in multi-RIS-aided multi-user mmWave/TeraHertz MIMO broadcast channel as a log determinant maximization problem, and propose phase iterative evolution (PIE) and water-filling segment matching (WSM) methods as solutions. PIE uses iterative coordinate ascent algorithm to solve the optimization problem where each iteration only updates phase-shift for one element of RIS with other elements being fixed, whereas WSM uses the asymptotic orthogonality of the array response vectors of mmWave/THz channel to develop a low-complexity solution. A joint hybrid precoding, hybrid combining and passive beamforming optimization problem is devised under max-min fairness criteria with total transmit power constraint in [32]. A sequential optimization technique is adopted to solve the joint optimization problem in which RIS phase-shift coefficients constrained to only taking finite equi-spaced quantized values of angles optimized by the alternating direction method of multipliers (ADMM).

In this article, point-to-point mmWave MIMO is considered in which the link between the BS and the user is blocked by an obstacle. To establish a link between the BS and the user, an RIS is deployed. The RIS elements only provide phase alterations to the incoming signal, so the RIS phase shift coefficients are constrained to have unit amplitudes. An iterative procedure is developed in which phase shift coefficients of the RIS are jointly designed with the precoder and the combiner. The developed design principle is applicable to both the narrowband and wideband scenarios. The contributions made in this article can be summarized as

(i) Considering the narrowband channel, RIS phase shift matrix is designed with the aim to minimize the mean square error (MSE) between the transmit signal and the estimate of the transmit signal at the receiver. The problem reduces to a quadratic problem in RIS phase shift vector which is equal to the diagonal of RIS phase shift matrix. The problem is in terms of precoding and combining matrices, which depends on RIS phase shift matrix. Thus, the problem can be solved to jointly determine RIS phase shift matrix, precoder and combiner. An iterative procedure is developed in which the solutions for each is computed in every iteration.
(ii) In particular, the passive beamforming subproblem is solved by extracting phases of the solution to unconstrained problem that ignores the unit modulus constraint of the reflecting elements of RIS. An equivalent optimization subproblem in RIS passive beamforming vector is defined to determine the low complexity solution to the unconstrained problem. The hybrid precoder is determined

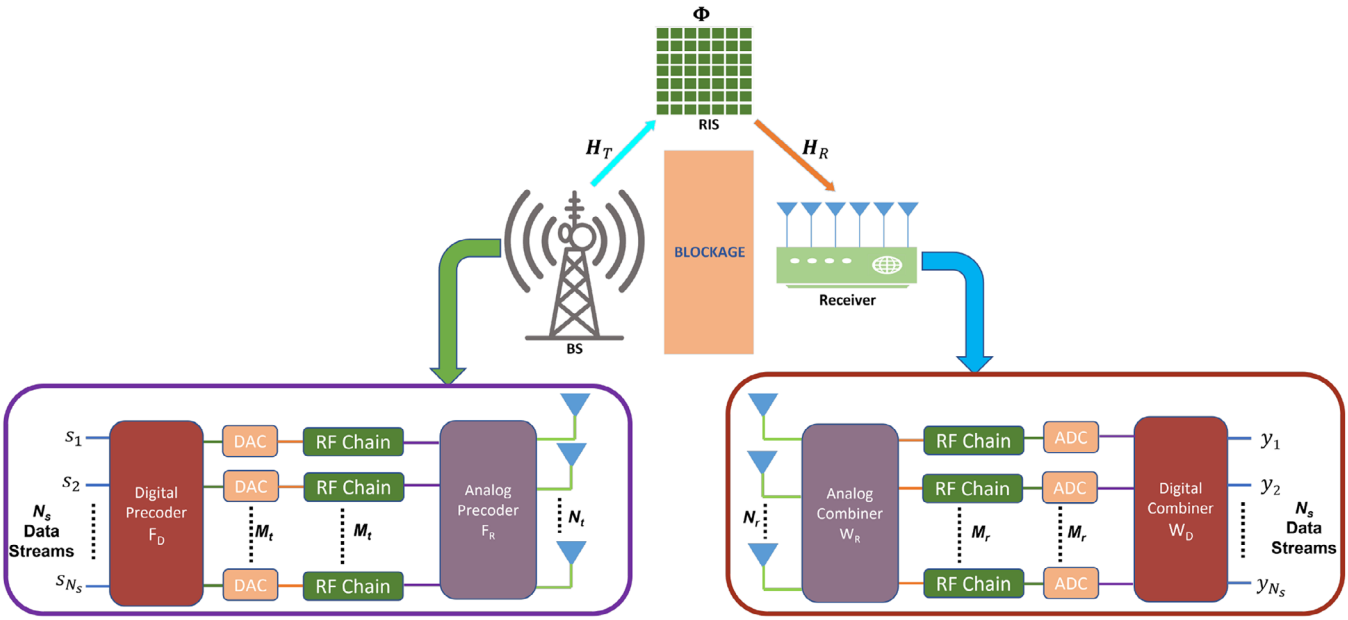


**FIGURE 1** mmWave MIMO with RIS-aided communication.

from the fully digital precoder after the RIS phase shift matrix is computed.

(iii) We then consider developing passive beamforming design for wideband channel with the application of orthogonal frequency division multiplexing (OFDM). The precoding and combining matrices are different for each OFDM subcarrier but the RIS phase shift matrix remains the same for all OFDM subcarriers. We show that the passive beamforming design method developed for the narrowband channel can be used to minimize the MSE of the system in wideband channel as well.

(iv) The complexity analysis of the proposed method is performed and compared against existing algorithms. Simulation results are generated to compare with the existing solutions. Comparison with the existing solutions shows that the proposed method gives high-grade performance which is better than state-of-the-art methods but entails lower complexity. We also show that the proposed method makes the condition of the channel better than the existing methods.

## 1.1 | Notations

$\mathbf{x}$ represents a vector, whereas $\mathbf{X}$ represents a matrix; $\mathbf{x}_i$ represents the $i$th element of $\mathbf{x}$; $\mathbf{X}_{i,j}$ represents the $(i,j)$th element of $\mathbf{X}$; $\mathbf{X}_{:,m:n}$ is a submatrix of $\mathbf{X}$ with all rows and columns $m$ to $n$; $\|\mathbf{x}\|_2$ is the $\ell 2$-norm of $\mathbf{x}$; $\|\mathbf{X}\|_F$ is the Frobenius norm of $\mathbf{X}$; $\mathbf{Tr}[\mathbf{X}]$ is the trace of $\mathbf{X}$; $\exp(\mathbf{X})$ is a matrix whose $(i,j)$th entry is $\exp\left(\mathbf{X}_{i,j}\right)$, where $\exp(.)$ is the exponential operator; $\mathbf{X}^{-1}$, $\mathbf{X}^{\dagger}$ and $\mathbf{X}^{H}$ are the inverse, pseudoinverse and Hermitian transpose of $\mathbf{X}$, respectively; $\odot$ is the Hadamard product of two matrices; $\mathbf{diag}(\mathbf{X})$ is a row vector containing the diagonal elements of $\mathbf{X}$; $\mathbf{DIAG}(a_1,\ldots,a_n)$ is an $n \times n$ diagonal matrix with $a_1,\ldots,a_n$ as the diagonal elements; $\mathbf{DIAG}(\mathbf{x})$ is a diagonal matrix with the elements of vector $\mathbf{x}$ as its diagonal elements; $\mathbf{I}_N$ is an $N \times N$ identity matrix; $\mathbb{R}_+$ denotes the set of positive real numbers; $\mathcal{O}$ represents the standard big-O notation; $\mathbb{E}[.]$ is the expectation operator; $\sim$ means 'has the probability distribution of'; $\triangleq$ means 'is defined as'; $\mathcal{CN}(\boldsymbol{\mu}, \mathbf{C})$ represents complex Gaussian vector with mean $\boldsymbol{\mu}$ and covariance matrix $\mathbf{C}$.

## 2 | SYSTEM MODEL

We consider a downlink point-to-point mmWave MIMO with $N_t$ antennas at the BS and $N_r$ antennas at the receiver, with the communication between the BS and the MS enhanced by an RIS with $N_I$ elements, as shown in Figure 1. We consider uniform planar array (UPA) of the RIS elements, whereas the uniform linear array (ULA) at the BS and the receiver. The precoding is accomplished at the base station by a hybrid precoder $\mathbf{F}$ which is a product of digital precoder $\mathbf{F}_{\mathrm{D}}, \mathbf{F}_{\mathrm{D}} \in \mathbb{C}^{M_t \times N_s}$ and analog precoder $\mathbf{F}_{\mathrm{R}}, \mathbf{F}_{\mathrm{R}} \in \mathbb{C}^{N_t \times M_t}$. At the receiver, combining is performed by a hybrid combiner $\mathbf{W} = \mathbf{W}_{\mathrm{R}}\mathbf{W}_{\mathrm{D}}$, where $\mathbf{W}_{\mathrm{R}} \in \mathbb{C}^{N_r \times M_r}$ and $\mathbf{W}_{\mathrm{D}} \in \mathbb{C}^{M_r \times N_s}$. We consider $N_t \geq N_r \geq M_t \geq M_r \geq N_s$, where $M_t$ and $M_r$ are the number of RF chains at the BS and the receiver, respectively, and $N_s$ is the number of data streams. The channel between the BS and the RIS is $\mathbf{H}_{\mathrm{T}}, \mathbf{H}_{\mathrm{T}} \in \mathbb{C}^{N_I \times N_t}$, the channel between the RIS and the receiver is $\mathbf{H}_{\mathrm{R}}, \mathbf{H}_{\mathrm{R}} \in \mathbb{C}^{N_r \times N_I}$, and the direct channel between the BS and the receiver is $\mathbf{H}_{\mathrm{D}} \in \mathbb{C}^{N_r \times N_t}$. The chances of direct link between the BS and the receiver not existing are very high in mmWave communication. This is true especially in urban or densely populated areas, where obstacles such as buildings, trees, or other structures can obstruct the direct Line of Sight (LoS) between BS and the receiver. Even though we assume that the direct channel does not exist between the BS and

the receiver, we consider $\mathbf{H}_{\text{D}}$ is non-zero for the time-being, for analysis purpose only. The signal impinging on the RIS is reflected after introducing phase shift $\boldsymbol{\phi}_i$ by $i$th element of the RIS. The RIS phase shift matrix $\boldsymbol{\Phi} = \mathbf{DIAG}(\boldsymbol{\phi}_1, \boldsymbol{\phi}_2, \dots, \boldsymbol{\phi}_{N_I})$. The equivalent channel between the BS and the receiver is given by [9, 27]

$$\mathbf{H} = \mathbf{H}_{\text{D}} + \mathbf{H}_{\text{R}}\boldsymbol{\Phi}\mathbf{H}_{\text{T}}. \tag{1}$$

The received signal is acted upon by the combiner $\mathbf{W}$ to yield the estimate of the transmit signal $\mathbf{s} \in \mathbb{C}^{N_s \times 1}$,

$$\mathbf{y} = \mathbf{W}^H\mathbf{H}\mathbf{F}\mathbf{s} + \mathbf{W}^H\mathbf{n}, \tag{2}$$

where $\mathbf{n} \in \mathbb{C}^{N_r \times 1}$ is noise vector such that $\mathbf{n} \sim \mathcal{CN}(\mathbf{0}, \sigma_n^2\mathbf{I}_{N_r})$. The channel between the BS and the RIS, and the channel from the RIS to the receiver are assumed narrowband and modeled by multi-path geometric channel model. The channel from the BS to the RIS and the channel from the RIS to the receiver are given by

$$\mathbf{H}_{\text{T}} = \sqrt{\frac{N_t N_I}{L_T}} \sum_{\ell=1}^{L_T} \alpha_\ell \mathbf{a}_{RIS}\left(\phi_\ell^{RIS,r}, \theta_\ell^{RIS,r}\right) \mathbf{a}_{BS}\left(\phi_\ell^{BS}\right)^H, \tag{3a}$$

$$\mathbf{H}_{\text{R}} = \sqrt{\frac{N_I N_r}{L_R}} \sum_{\ell=1}^{L_R} \beta_\ell \mathbf{a}_R\left(\phi_\ell^{R}\right) \mathbf{a}_{RIS}\left(\phi_\ell^{RIS,t}, \theta_\ell^{RIS,t}\right)^H, \tag{3b}$$

where $\mathbf{a}_{RIS}(\phi_\ell^{RIS}, \theta_\ell^{RIS})$, $\mathbf{a}_{BS}(\phi_\ell^{BS})$ and $\mathbf{a}_R(\phi_\ell^R)$ are antenna array response vectors of the RIS, the BS and the receiver, respectively, while $L_T$ and $L_R$ represent the number of paths in transmitter-RIS link and RIS-receiver link, respectively. $\phi_\ell^{RIS,r}(\theta_\ell^{RIS,r})$, $\phi_\ell^{BS}$, $\phi_\ell^{RIS,t}(\theta_\ell^{RIS,t})$ and $\phi_\ell^R$ are the azimuth (elevation) angles of arrival at the RIS, azimuth angles of departure at the BS, azimuth (elevation) angles of departure at the RIS and azimuth angles of arrival at the receiver, respectively. The antenna array response vectors of ULA with $N$ antennas and UPA with $N_y \times N_z$ antennas are given by

$$\mathbf{a}(\phi) = \frac{1}{\sqrt{N}}\begin{bmatrix} 1 & e^{j\zeta d(\sin\phi)} & \dots & e^{j\zeta d((N-1)\sin\phi)} \end{bmatrix}^T, \tag{4a}$$

$$\mathbf{a}(\phi, \theta) = \frac{1}{\sqrt{N_y N_z}}\Big[1 \ \dots \ e^{j\zeta d(y\sin\phi\sin\theta + z\cos\theta)} \ \dots \ e^{j\zeta d((N_y-1)\sin\phi\sin\theta + (N_z-1)\cos\theta)}\Big]^T, \tag{4b}$$

where $\zeta = \frac{2\pi}{\lambda}$, $\lambda$ being the carrier wavelength, and $d$ is the distance between antenna elements.

## 3 | PROBLEM STATEMENT

We determine the phase shift matrix for the RIS $\boldsymbol{\Phi}$ and the precoder in two different stages. We assume that the channel matrices $\mathbf{H}_{\text{R}}$, $\mathbf{H}_{\text{T}}$ and $\mathbf{H}_{\text{D}}$ are known. We first determine $\boldsymbol{\Phi}$ and then compute the hybrid precoder once $\boldsymbol{\Phi}$ is fixed. For the sake of simplicity, we consider fully digital precoder $\mathbf{F}_{\text{FD}}$ and fully digital combiner $\mathbf{W}_{\text{FD}}$ at both the transmitter and the receiver to determine the phase shift matrix for the RIS.

### 3.1 | Passive beamforming problem

In this section, we define the problem for RIS phase-shift matrix, also known as passive beamforming matrix, determination. We consider the MSE between the transmit signal $\mathbf{s}$ and the combined received signal $\mathbf{y}$ at the receiver,

$$\text{MSE} = \mathbb{E}\left[\|\mathbf{s} - \mathbf{y}\|_2^2\right]. \tag{5}$$

We minimize MSE to determine $\boldsymbol{\Phi}$. Since $\mathbb{E}[\mathbf{s}\mathbf{s}^H] = \mathbf{I}_{N_s}$, the MSE can be written after substituting the expression for $\mathbf{y}$ as

$$\begin{aligned}\text{MSE} = \mathbf{Tr}\big[&\mathbf{I} - \mathbf{W}_{\text{FD}}^H\mathbf{H}\mathbf{F}_{\text{FD}} - \mathbf{F}_{\text{FD}}^H\mathbf{H}^H\mathbf{W}_{\text{FD}} \\ &+ \mathbf{W}_{\text{FD}}^H\mathbf{H}\mathbf{F}_{\text{FD}}\mathbf{F}_{\text{FD}}^H\mathbf{H}^H\mathbf{W}_{\text{FD}} + \sigma_n^2\mathbf{W}_{\text{FD}}^H\mathbf{W}_{\text{FD}}\big].\end{aligned} \tag{6}$$

Similar to [19] which converts the weighted minimum mean square error (WMMSE) problem in terms of passive beamforming vector, we also express the MMSE problem in terms of passive beamforming vector by substituting $\mathbf{H} = \mathbf{H}_{\text{R}}\boldsymbol{\Phi}\mathbf{H}_{\text{T}}$ in the expression for MSE and simplifying as

$$\text{MSE} = \boldsymbol{\phi}\mathbf{C}\boldsymbol{\phi}^H - \boldsymbol{\phi}\mathbf{t} - \mathbf{t}^H\boldsymbol{\phi}^H + N_s + \sigma_n^2 w + u, \text{where} \tag{7a}$$

$$\mathbf{C}_1 \triangleq \mathbf{H}_{\text{T}}\mathbf{F}_{\text{FD}}\mathbf{F}_{\text{FD}}^H\mathbf{H}_{\text{T}}^H, \tag{7b}$$

$$\mathbf{C}_2 \triangleq \mathbf{H}_{\text{R}}^H\mathbf{W}_{\text{FD}}\mathbf{W}_{\text{FD}}^H\mathbf{H}_{\text{R}}, \tag{7c}$$

$$\mathbf{t} \triangleq \mathbf{diag}\big(\mathbf{H}_{\text{T}}\mathbf{F}_{\text{FD}}\mathbf{W}_{\text{FD}}^H\mathbf{H}_{\text{R}} - \mathbf{H}_{\text{T}}\mathbf{F}_{\text{FD}}\mathbf{F}_{\text{FD}}^H\mathbf{H}_{\text{D}}^H\mathbf{W}_{\text{FD}}\mathbf{W}_{\text{FD}}^H\mathbf{H}_{\text{R}}\big), \tag{7d}$$

$$\mathbf{C} \triangleq \mathbf{C}_1 \odot \mathbf{C}_2^T, \tag{7e}$$

$$\boldsymbol{\phi} \triangleq \mathbf{diag}(\boldsymbol{\Phi}), \boldsymbol{\phi} \in \mathbb{C}^{1\times N_I}. \tag{7f}$$

$$w \triangleq \mathbf{Tr}\left[\mathbf{W}_{\text{FD}}^H\mathbf{W}_{\text{FD}}\right], \quad \text{and} \tag{7g}$$

$$\begin{aligned}u \triangleq \mathbf{Tr}\big[&\mathbf{W}_{\text{FD}}^H\mathbf{H}_{\text{D}}\mathbf{F}_{\text{FD}}\mathbf{F}_{\text{FD}}^H\mathbf{H}_{\text{D}}^H\mathbf{W}_{\text{FD}} - \mathbf{W}_{\text{FD}}^H\mathbf{H}_{\text{D}}\mathbf{F}_{\text{FD}} \\ &- \mathbf{F}_{\text{FD}}^H\mathbf{H}_{\text{D}}^H\mathbf{W}_{\text{FD}}\big].\end{aligned} \tag{7h}$$

Instead of $\boldsymbol{\Phi}$ itself, the expression for MSE is now in terms of row vector $\boldsymbol{\phi}$. The problem of determining optimal $\boldsymbol{\phi}$ and hence $\boldsymbol{\Phi}$, can be stated as

$$\boldsymbol{\phi}^\star = \arg\min_{\boldsymbol{\phi}} \ \boldsymbol{\phi}\mathbf{C}\boldsymbol{\phi}^H - \boldsymbol{\phi}\mathbf{t} - \mathbf{t}^H\boldsymbol{\phi}^H + \left(N_s + \sigma_n^2 w + u\right), \tag{8a}$$

$$\text{s.t.} \quad |\boldsymbol{\phi}_i| = 1, \quad \forall i = 1, \dots, N_I. \tag{8b}$$

$$
\begin{aligned}
\text{MSE} &= \mathbf{Tr}\big[\mathbf{I} - \mathbf{W}_{\text{FD}}^H\mathbf{H}_{\text{D}}\mathbf{F}_{\text{FD}} - \mathbf{W}_{\text{FD}}^H\mathbf{H}_{\text{R}}\boldsymbol{\Phi}\mathbf{H}_{\text{T}}\mathbf{F}_{\text{FD}} - \mathbf{F}_{\text{FD}}^H\mathbf{H}_{\text{T}}^H\boldsymbol{\Phi}^H\mathbf{H}_{\text{R}}^H\mathbf{W}_{\text{FD}} - \mathbf{F}_{\text{FD}}^H\mathbf{H}_{\text{D}}^H\mathbf{W}_{\text{FD}} + \mathbf{W}_{\text{FD}}^H\mathbf{H}_{\text{R}}\boldsymbol{\Phi}\mathbf{H}_{\text{T}}\mathbf{F}_{\text{FD}}\mathbf{F}_{\text{FD}}^H\mathbf{H}_{\text{T}}^H\boldsymbol{\Phi}^H\mathbf{H}_{\text{R}}^H \\
&\quad \mathbf{W}_{\text{FD}} + \mathbf{W}_{\text{FD}}^H\mathbf{H}_{\text{R}}\boldsymbol{\Phi}\mathbf{H}_{\text{T}}\mathbf{F}_{\text{FD}}\mathbf{F}_{\text{FD}}^H\mathbf{H}_{\text{D}}^H\mathbf{W}_{\text{FD}} + \mathbf{W}_{\text{FD}}^H\mathbf{H}_{\text{D}}\mathbf{F}_{\text{FD}}\mathbf{F}_{\text{FD}}^H\mathbf{H}_{\text{T}}^H\boldsymbol{\Phi}^H\mathbf{H}_{\text{R}}^H\mathbf{W}_{\text{FD}} + \mathbf{W}_{\text{FD}}^H\mathbf{H}_{\text{D}}\mathbf{F}_{\text{FD}}\mathbf{F}_{\text{FD}}^H\mathbf{H}_{\text{D}}^H\mathbf{W}_{\text{FD}} + \sigma_n^2\mathbf{W}_{\text{FD}}^H\mathbf{W}_{\text{FD}}\big] \\
&= \mathbf{Tr}\big[\boldsymbol{\Phi}\big(\mathbf{H}_{\text{T}}\mathbf{F}_{\text{FD}}\mathbf{F}_{\text{FD}}^H\mathbf{H}_{\text{T}}^H\big)\boldsymbol{\Phi}^H\big(\mathbf{H}_{\text{R}}^H\mathbf{W}_{\text{FD}}\mathbf{W}_{\text{FD}}^H\mathbf{H}_{\text{R}}\big) + \boldsymbol{\Phi}\big(\mathbf{H}_{\text{T}}\mathbf{F}_{\text{FD}}\mathbf{F}_{\text{FD}}^H\mathbf{H}_{\text{D}}^H\mathbf{W}_{\text{FD}}\mathbf{W}_{\text{FD}}^H\mathbf{H}_{\text{R}}\big) - \boldsymbol{\Phi}\big(\mathbf{H}_{\text{T}}\mathbf{F}_{\text{FD}}\mathbf{W}_{\text{FD}}^H\mathbf{H}_{\text{R}}\big) - \\
&\quad \big(\mathbf{H}_{\text{R}}^H\mathbf{W}_{\text{FD}}\mathbf{F}_{\text{FD}}^H\mathbf{H}_{\text{T}}^H\big)\boldsymbol{\Phi}^H + \big(\mathbf{H}_{\text{R}}^H\mathbf{W}_{\text{FD}}\mathbf{W}_{\text{FD}}^H\mathbf{H}_{\text{D}}\mathbf{F}_{\text{FD}}\mathbf{F}_{\text{FD}}^H\mathbf{H}_{\text{T}}^H\big)\boldsymbol{\Phi}^H\big] + \mathbf{Tr}\big[\mathbf{I} + \mathbf{W}_{\text{FD}}^H\mathbf{H}_{\text{D}}\mathbf{F}_{\text{FD}}\mathbf{F}_{\text{FD}}^H\mathbf{H}_{\text{D}}^H\mathbf{W}_{\text{FD}} - \mathbf{W}_{\text{FD}}^H\mathbf{H}_{\text{D}}\mathbf{F}_{\text{FD}} - \\
&\quad \mathbf{F}_{\text{FD}}^H\mathbf{H}_{\text{D}}^H\mathbf{W}_{\text{FD}} + \sigma_n^2\mathbf{W}_{\text{FD}}^H\mathbf{W}_{\text{FD}}\big] \\
&= \mathbf{Tr}\big[\boldsymbol{\Phi}\big(\mathbf{H}_{\text{T}}\mathbf{F}_{\text{FD}}\mathbf{F}_{\text{FD}}^H\mathbf{H}_{\text{T}}^H\big)\boldsymbol{\Phi}^H\big(\mathbf{H}_{\text{R}}^H\mathbf{W}_{\text{FD}}\mathbf{W}_{\text{FD}}^H\mathbf{H}_{\text{R}}\big) - \boldsymbol{\Phi}\big(\mathbf{H}_{\text{T}}\mathbf{F}_{\text{FD}}\mathbf{W}_{\text{FD}}^H\mathbf{H}_{\text{R}} - \mathbf{H}_{\text{T}}\mathbf{F}_{\text{FD}}\mathbf{F}_{\text{FD}}^H\mathbf{H}_{\text{D}}^H\mathbf{W}_{\text{FD}}\mathbf{W}_{\text{FD}}^H\mathbf{H}_{\text{R}}\big) - \\
&\quad \big(\mathbf{H}_{\text{R}}^H\mathbf{W}_{\text{FD}}\mathbf{F}_{\text{FD}}^H\mathbf{H}_{\text{T}}^H - \mathbf{H}_{\text{R}}^H\mathbf{W}_{\text{FD}}\mathbf{W}_{\text{FD}}^H\mathbf{H}_{\text{D}}\mathbf{F}_{\text{FD}}\mathbf{F}_{\text{FD}}^H\mathbf{H}_{\text{T}}^H\big)\boldsymbol{\Phi}^H\big] + \mathbf{Tr}\big[\mathbf{I} + \mathbf{W}_{\text{FD}}^H\mathbf{H}_{\text{D}}\mathbf{F}_{\text{FD}}\mathbf{F}_{\text{FD}}^H\mathbf{H}_{\text{D}}^H\mathbf{W}_{\text{FD}} - \mathbf{W}_{\text{FD}}^H\mathbf{H}_{\text{D}}\mathbf{F}_{\text{FD}} - \\
&\quad \mathbf{F}_{\text{FD}}^H\mathbf{H}_{\text{D}}^H\mathbf{W}_{\text{FD}} + \sigma_n^2\mathbf{W}_{\text{FD}}^H\mathbf{W}_{\text{FD}}\big] \\
&\overset{a}{=} \boldsymbol{\phi}\big(\mathbf{C}_1 \odot \mathbf{C}_2^T\big)\boldsymbol{\phi}^H - \boldsymbol{\phi}\mathbf{t} - \mathbf{t}^H\boldsymbol{\phi}^H + \mathbf{Tr}\big[\mathbf{I} + \sigma_n^2\mathbf{W}_{\text{FD}}^H\mathbf{W}_{\text{FD}}\big] + \mathbf{Tr}\big[\mathbf{W}_{\text{FD}}^H\mathbf{H}_{\text{D}}\mathbf{F}_{\text{FD}}\mathbf{F}_{\text{FD}}^H\mathbf{H}_{\text{D}}^H\mathbf{W}_{\text{FD}}\mathbf{W}_{\text{FD}}^H\mathbf{H}_{\text{D}}\mathbf{F}_{\text{FD}} - \mathbf{F}_{\text{FD}}^H\mathbf{H}_{\text{D}}^H\mathbf{W}_{\text{FD}}\big]
\end{aligned}
$$

The reasons behind $(a)$ are matrix identities $\mathbf{Tr}\big[\boldsymbol{\Phi}\mathbf{C}_1\boldsymbol{\Phi}^H\mathbf{C}_2\big] = \boldsymbol{\phi}\big(\mathbf{C}_1 \odot \mathbf{C}_2^T\big)\boldsymbol{\phi}^H$ and $\mathbf{Tr}[\boldsymbol{\Phi}\mathbf{T}] = \boldsymbol{\phi}\mathbf{diag}(\mathbf{T})$ for the diagonal matrix $\boldsymbol{\Phi}$ [33], where $\boldsymbol{\phi}$ is a row vector corresponding to the diagonal of diagonal matrix $\boldsymbol{\Phi}$.

The solution to the problem (8) is difficult because the constraint (8b) is non-convex, and there is no known optimal solution to the problem (8). The problem similar to (8) can be solved by performing optimization on the complex circle manifold, similar to the algorithm proposed in [34]. However, we develop our own algorithm to solve the problem (8) which not only produces better performance but also entails low complexity.

## 3.2 | Hybrid precoding problem

A careful look at the optimization problem (8) shows that $\boldsymbol{\Phi}$ or $\boldsymbol{\phi}$ depends on $\mathbf{F}_{\text{FD}}$ and $\mathbf{W}_{\text{FD}}$. If there is a knowledge about channel matrix $\mathbf{H}$, the fully digital precoder for point-to-point MIMO can be calculated as

$$\mathbf{F}_{\text{FD}} = \mathbf{V}_{:,1:N_s}\boldsymbol{\Gamma}_{\text{FD}}, \quad \text{and} \tag{9a}$$

$$\boldsymbol{\Gamma}_{\text{FD}} = \mathbf{DIAG}\left(\sqrt{p_1}, \sqrt{p_2}, \dots, \sqrt{p_{N_s}}\right), \tag{9b}$$

where $\boldsymbol{\Gamma}_{\text{FD}}$ is the power loading matrix, $\mathbf{H} = \mathbf{U}\boldsymbol{\Sigma}\mathbf{V}^H$ is the SVD of channel matrix $\mathbf{H}$, and $p_i, \forall i = 1, 2, \dots, N_s$ is the power along the $i$th data stream. The optimal $\boldsymbol{\Gamma}_{\text{FD}}$ is computed by the water-filling solution, whereas $\boldsymbol{\Gamma}_{\text{FD}} = \frac{P}{N_s}\mathbf{I}_{N_s}$ in case of equal power distribution, $P$ being the maximum total transmit power. On the other hand, the fully digital combiner at the receiver is given by the MMSE combiner,

$$\mathbf{W}_{\text{FD}} = \big(\mathbf{H}\mathbf{F}_{\text{FD}}\mathbf{F}_{\text{FD}}^H\mathbf{H}^H + \sigma_n^2\mathbf{I}_{N_r}\big)^{-1}\mathbf{H}\mathbf{F}_{\text{FD}}. \tag{10}$$

The hybrid precoder is computed by minimizing the Euclidean distance from its fully digital counterpart, $\mathbf{F}_{\text{FD}}$. The hybrid precoding problem [35] is stated as

$$\underset{\mathbf{F}_{\text{R}},\mathbf{F}_{\text{D}}}{\arg\min} \quad \left\|\mathbf{F}_{\text{FD}} - \mathbf{F}_{\text{R}}\mathbf{F}_{\text{D}}\right\|_F^2, \tag{11a}$$

$$\text{s.t.} \quad \|\mathbf{F}_{\text{R}}\mathbf{F}_{\text{D}}\|_F^2 = N_s, \tag{11b}$$

$$\left|\mathbf{F}_{\text{R}_{i,j}}\right| = 1, \ \forall i, j. \tag{11c}$$

We determine $\mathbf{F}_{\text{R}}$ and $\mathbf{F}_{\text{D}}$ in two separate stages; $\mathbf{F}_{\text{R}}$ is determined first, followed by computation of $\mathbf{F}_{\text{D}}$ for fixed $\mathbf{F}_{\text{R}}$. In [36], we show that two-stage hybrid precoder can be determined by first solving analog precoding subproblem,

$$\underset{\mathbf{F}_{\text{R}}}{\arg\max} \quad \mathbf{Tr}\big[\mathbf{F}_{\text{R}}^H\mathbf{F}_{\text{FD}}\mathbf{F}_{\text{FD}}^H\mathbf{F}_{\text{R}}\big], \tag{12a}$$

$$\text{s.t.} \quad \left|\mathbf{F}_{\text{R}_{i,j}}\right| = 1, \quad \forall i, j, \tag{12b}$$

$$\mathbf{F}_{\text{R}}^H\mathbf{F}_{\text{R}} = N_t\mathbf{I}_{\text{M}_t}. \tag{12c}$$

After $\mathbf{F}_{\text{R}}$ is evaluated, $\mathbf{F}_{\text{D}}$ is computed as [36],

$$\mathbf{F}_{\text{D}} = \beta_F\mathbf{F}_{\text{R}}^{\dagger}\mathbf{F}_{\text{FD}}, \quad \text{where} \tag{13a}$$

$$\beta_F = \frac{\sqrt{N_s}}{\|\mathbf{F}_{\text{R}}^{\dagger}\mathbf{F}_{\text{FD}}\|_F}, \tag{13b}$$

where $\beta_F$ is the normalization factor arising due to the power constraint (11b). We can also compute $\mathbf{F}_{\text{D}}$ as the matrix containing right singular vectors corresponding to the leading $N_s$

eigenvalues of the matrix $\mathbf{HF}_{\mathrm{R}}$. The hybrid combining problem is similar to hybrid precoding problem (11) but devoid of the power constraint as in (11b). Thus, the only difference in the solution of hybrid combiner from hybrid precoder is that the digital combiner does not have a normalization factor.

## 4 | PROPOSED SOLUTION

We solve $\boldsymbol{\Phi}$ by solving the problem given by (8). The objective function (8a) is dependent on the values of $\mathbf{F}_{\mathrm{FD}}$ and $\mathbf{W}_{\mathrm{FD}}$ which are given by Equations (9a) and (10), and can be computed if $\mathbf{H}$ is known. Hence, $\mathbf{F}_{\mathrm{FD}}$ and $\mathbf{W}_{\mathrm{FD}}$ are themselves dependent on $\boldsymbol{\Phi}$ as the value of $\mathbf{H}$ is determined by $\boldsymbol{\Phi}$.

### 4.1 | Passive beamforming subproblem

There is no known optimal solution to the problem (8) to the best of authors' knowledge. Problem (8) can be modeled as a Boolean quadratic programming problem. Boolean quadratic program is computationally difficult as it belongs to the class of NP-hard problems [37]. We can, however, translate such problems into a semidefinite programming problem [37] after semidefinite relaxation [38]. But the solution is still computationally demanding. In pursuit of simpler solution, we determine the optimal $\boldsymbol{\phi}$ by extracting the phases of the vector $\boldsymbol{\phi}_{uc}$, the optimal solution to the problem (8) without taking the constraint (8b) into account. Each element of $\boldsymbol{\phi}_{uc}$ is not constrained to satisfy unit modulus constraint. Taking derivative of the objective function (8a) and equating it to zero gives the solution for $\boldsymbol{\phi}_{uc}$. But it is in terms of $\mathbf{C}^{-1}$, and for $\mathbf{C}^{-1}$ to exist, $\mathbf{C}$ should be full-rank which cannot be guaranteed. To get around this problem, we consider another optimization problem,

$$\boldsymbol{\phi}^{\star} = \arg\min_{\boldsymbol{\phi}} \quad \boldsymbol{\phi}(\mathbf{C}+\mu\mathbf{I})\boldsymbol{\phi}^{H} - \boldsymbol{\phi}\mathbf{t} - \mathbf{t}^{H}\boldsymbol{\phi}^{H}, \tag{14a}$$

$$\text{s.t.} \quad |\boldsymbol{\phi}_i| = 1, \quad \forall i, \tag{14b}$$

where $\mu \in \mathbb{R}_{+}$. The unconstrained optimal solution to the problem (14), $\boldsymbol{\phi}_{uc}$ is obtained by taking derivative of the objective function (14a) with respect to $\boldsymbol{\phi}$ and equating to 0,

$$\boldsymbol{\phi}_{uc} = \mathbf{t}^{H}(\mathbf{C}+\mu\mathbf{I})^{-1}, \tag{15}$$

where $\mathbf{C}+\mu\mathbf{I}$ is always a full-rank matrix. Let us simplify the objective function (14a) as

$$\begin{aligned}
&\boldsymbol{\phi}(\mathbf{C}+\mu\mathbf{I})\boldsymbol{\phi}^{H} - \boldsymbol{\phi}\mathbf{t} - \mathbf{t}^{H}\boldsymbol{\phi}^{H} \\
&= \boldsymbol{\phi}\mathbf{C}\boldsymbol{\phi}^{H} + \mu\boldsymbol{\phi}\boldsymbol{\phi}^{H} - \boldsymbol{\phi}\mathbf{t} - \mathbf{t}^{H}\boldsymbol{\phi}^{H} \\
&= \boldsymbol{\phi}\mathbf{C}\boldsymbol{\phi}^{H} + \mu\sum_{i=1}^{N_I}|\boldsymbol{\phi}_i|^2 - \boldsymbol{\phi}\mathbf{t} - \mathbf{t}^{H}\boldsymbol{\phi}^{H} \\
&= \boldsymbol{\phi}\mathbf{C}\boldsymbol{\phi}^{H} + \mu N_I - \boldsymbol{\phi}\mathbf{t} - \mathbf{t}^{H}\boldsymbol{\phi}^{H}.
\end{aligned}$$

**ALGORITHM 1** MMSE-based passive beamforming design method.

**Require**: $\mathbf{H}_{\mathrm{T}}, \mathbf{H}_{\mathrm{R}}, N_s, N_I, P$.

1: Choose initial value of $\boldsymbol{\phi}^{(0)}$ randomly such that $\left|\boldsymbol{\phi}_i^{(0)}\right| = 1$ so that $\boldsymbol{\Phi}^{(0)} = \mathbf{diag}\left(\boldsymbol{\phi}^{(0)}\right)$ and $\mathbf{H}^{(0)} = \mathbf{H}_{\mathrm{R}}\boldsymbol{\Phi}^{(0)}\mathbf{H}_{\mathrm{T}}$.
2: Set $\epsilon = 10^{-4}$, a very small value, and set $k \leftarrow 1$.
3: **repeat**
4: Compute $\mathbf{F}_{\mathrm{FD}}^{(k)}$, using (9).
5: Compute $\mathbf{W}_{\mathrm{FD}}^{(k)}$ using (10).
6: Compute $\boldsymbol{\phi}^{(k)}$ using (17). Set $\boldsymbol{\Phi}^{(k)} = \mathbf{DIAG}\left(\boldsymbol{\phi}^{(k)}\right)$.
7: Set $\mathbf{H}^{(k)} = \mathbf{H}_{\mathrm{R}}\boldsymbol{\Phi}^{(k)}\mathbf{H}_{\mathrm{T}}$.
8: Compute $\mathrm{MSE}^{(k)}$ using (6).
9: Compute $\delta^{(k)} = \left|\mathrm{MSE}^{(k)} - \mathrm{MSE}^{(k-1)}\right|$.
10: Set $k \leftarrow k+1$.
11: **until** $\delta^{(k)} < \epsilon$
12: $\boldsymbol{\Phi} = \boldsymbol{\Phi}^{(k)}$, $\mathbf{H} = \mathbf{H}^{k}$.
13: Compute $\mathbf{F}_{\mathrm{FD}}^{(k)}$ using (9) and compute $\mathbf{W}_{\mathrm{FD}}$ using (10).
14: **return** $\boldsymbol{\Phi}, \mathbf{H}, \mathbf{F}_{\mathrm{FD}}, \mathbf{W}_{\mathrm{FD}}$.

The objective functions (8a) and (14a) are equivalent when

$$\mu = \frac{1}{N_I}\left(N_s + \sigma_n^2 w + u\right). \tag{16}$$

Thus, we determine $\boldsymbol{\phi}$ by normalizing each element of $\boldsymbol{\phi}_{uc}$ to have unit amplitude as

$$\boldsymbol{\phi} = \exp\left(j\angle\left(\mathbf{t}^{H}(\mathbf{C}+\mu\mathbf{I})^{-1}\right)\right), \tag{17}$$

where $\mu$ is given by (16). The phase-shifts rendered by the RIS elements are not continuous but discrete which can be characterized by $B$ quantization bits. Thus, the continuous phase values need to be quantized to realize them practically. The quantized phase $\phi_q$ can be obtained by quantizing the unquantized phase value $\phi_{uq}$ to $B$ values of precision as [39]

$$\phi_q = \frac{2\pi n}{2^B}, \tag{18a}$$

$$\text{where} \quad n = \arg\min_{m \in \{0,\ldots,2^B-1\}}\left|\phi_{uq} - \frac{2\pi m}{2^B}\right|. \tag{18b}$$

### 4.2 | Passive beamforming solution based on iterative method

Once $\boldsymbol{\phi}$ is calculated, $\mathbf{H}$ is known and both $\mathbf{F}_{\mathrm{FD}}$ and $\mathbf{W}_{\mathrm{FD}}$ can be computed. An iterative procedure is developed where $\boldsymbol{\phi}$ is initialized with a random value, so that there is an initial value of $\mathbf{H}$. At each iteration, the SVD of $\mathbf{H}$ is performed, and the leading $N_s$ right singular vectors serve as the solution for $\mathbf{F}_{\mathrm{FD}}$, as in (9a). $\mathbf{W}_{\mathrm{FD}}$ is computed using (10), as $\mathbf{H}$ and $\mathbf{F}_{\mathrm{FD}}$ are known. Finally, $\boldsymbol{\phi}$ is determined using (17). This procedure is repeated until convergence is reached. The summary of the algorithm to determine $\boldsymbol{\phi}$ is presented in Algorithm 1.

### 4.3 | Hybrid precoding solution

We define $\bar{\mathbf{F}}_{\mathrm{R}} \triangleq \frac{1}{\sqrt{N_t}}\mathbf{F}_{\mathrm{R}}$ and rewrite the optimization problem (12) in terms of $\bar{\mathbf{F}}_{\mathrm{R}}$ as

$$\max_{\bar{\mathbf{F}}_{\mathrm{R}}} \quad \mathbf{Tr}\left[\bar{\mathbf{F}}_{\mathrm{R}}^{H}\left(\mathbf{F}_{\mathrm{FD}}\mathbf{F}_{\mathrm{FD}}^{H}\right)\bar{\mathbf{F}}_{\mathrm{R}}\right], \tag{19a}$$

$$\text{s.t.} \quad \left|\bar{\mathbf{F}}_{\mathrm{R}_{i,j}}\right| = \frac{1}{\sqrt{N_t}},\ \forall i,j, \tag{19b}$$

$$\bar{\mathbf{F}}_{\mathrm{R}}^{H}\bar{\mathbf{F}}_{\mathrm{R}} = \mathbf{I}_{\mathrm{M}_t}. \tag{19c}$$

We compute $\mathbf{F}_{\mathrm{R}}$ as $\mathbf{F}_{\mathrm{R}} = \sqrt{N_t}\bar{\mathbf{F}}_{\mathrm{R}}$ after solving the problem (19). We use the iterative SVD-based procedure proposed in [40] to solve the problem (19). For the sake of completion, we describe the method in full. The trace $\mathbf{Tr}\left[\bar{\mathbf{F}}_{\mathrm{R}}^{H}\left(\mathbf{F}_{\mathrm{FD}}\mathbf{F}_{\mathrm{FD}}^{H}\right)\bar{\mathbf{F}}_{\mathrm{R}}\right]$ is always real and positive because $\mathbf{F}_{\mathrm{FD}}\mathbf{F}_{\mathrm{FD}}^{H}$ is a Hermitian positive-semidefinite matrix. The objective function (19a) can be equivalently substituted by $\left|\mathbf{Tr}\left[\bar{\mathbf{F}}_{\mathrm{R}}^{H}\left(\mathbf{F}_{\mathrm{FD}}\mathbf{F}_{\mathrm{FD}}^{H}\right)\bar{\mathbf{F}}_{\mathrm{R}}\right]\right|$.

We initialize $\bar{\mathbf{F}}_{\mathrm{R}}^{(0)}$ with a valid, but random initial value. We define a new matrix $\mathbf{A}^{(k)} \triangleq \bar{\mathbf{F}}_{\mathrm{R}}^{(k-1)^{H}}\left(\mathbf{F}_{\mathrm{FD}}\mathbf{F}_{\mathrm{FD}}^{H}\right)$, where $k$ is the iteration index starting from 1. At the $k$th iteration, we determine the solution to the problem,

$$\begin{aligned} &\arg\max_{\mathbf{D}^{(k)}} \ |\mathbf{Tr}(\mathbf{A}^{(k)}\mathbf{D}^{(k)})| \\ &s.t. \quad \mathbf{D}^{(k)^{H}}\mathbf{D}^{(k)} = \mathbf{I}_{M_t}. \end{aligned} \tag{20}$$

The optimal solution to the problem (17) is $\mathbf{D}^{(k)} = \mathbf{V}_t^{(k)}\mathbf{U}^{(k)^{H}}$, where $\mathbf{A}^{(k)} = \mathbf{U}^{(k)}\mathbf{S}^{(k)}\mathbf{V}_t^{(k)^{H}}$ is the truncated SVD of $\mathbf{A}^{(k)}$. $\bar{\mathbf{F}}_{\mathrm{R}}^{(k)}$ is approximated by extracting phase of each element of the matrix $\mathbf{D}^{(k)}$, and enforcing each element to have an amplitude of $\frac{1}{\sqrt{N_t}}$.

We update the iteration index and determine the new value of $\mathbf{A}^{(k)}$. This procedure is repeated until we reach the convergence, or perform a fixed number of iterations. Finally, $\mathbf{F}_{\mathrm{R}}$ is computed as $\mathbf{F}_{\mathrm{R}} = \sqrt{N_t}\bar{\mathbf{F}}_{\mathrm{R}}$. Once we have computed $\mathbf{F}_{\mathrm{R}}$, the digital precoder $\mathbf{F}_{\mathrm{D}}$ is determined using (13). The outline of the proposed algorithm is presented in Algorithm 2.

**ALGORITHM 2** SVD-based iterative trace maximization method.

**Require**: $\mathbf{F}_{\mathrm{FD}}, M_t$.

1: Initialize $\bar{\mathbf{F}}_{\mathrm{R}}^{(0)} = \frac{1}{\sqrt{N_t}}\exp(j\boldsymbol{\Theta})$, where $\boldsymbol{\Theta}$ is $N_t \times M_t$ matrix and $\boldsymbol{\Theta}_{i,j}$ are random phase angles, and set $k = 1$.
2: **repeat**
3: Compute $\mathbf{A}^{(k)} = \bar{\mathbf{F}}_{\mathrm{R}}^{(k-1)^{H}}\left(\mathbf{F}_{\mathrm{FD}}\mathbf{F}_{\mathrm{FD}}^{H}\right)$.
4: Compute truncated SVD: $\mathbf{A}^{(k)} = \mathbf{U}^{(k)}\mathbf{S}^{(k)}\mathbf{V}_t^{(k)^{H}}$.
5: Compute $\mathbf{D}^{(k)} = \mathbf{V}_t^{(k)}\mathbf{U}^{(k)^{H}}$.
6: Compute $\bar{\mathbf{F}}_{\mathrm{R}}^{(k)} = \frac{1}{\sqrt{N_t}}\exp\left(j\angle\left(\mathbf{D}^{(k)}\right)\right)$.
7: $k \leftarrow k + 1$.
8: **until** convergence, or $k \geq iter_{max}$, where $iter_{max}$ is the maximum of number of iterations.
9: Compute $\mathbf{F}_{\mathrm{R}} = \sqrt{N_t}\bar{\mathbf{F}}_{\mathrm{R}}^{(k)}$.
10: Calculate $\mathbf{F}_{\mathrm{D}}$, using (13).
11: **return** $\mathbf{F} = \mathbf{F}_{\mathrm{R}}\mathbf{F}_{\mathrm{D}}$.

## 5 | EXTENSION TO WIDEBAND CHANNEL

### 5.1 | Passive beamforming for wideband channel

The proposed solution for passive beamforming can also be applied in wideband scenario by considering transmission over frequency selective channels using MIMO-OFDM. The hybrid precoder (combiner) in wideband MIMO-OFDM system constitutes of different digital precoders (combiners) for each of the subcarriers and an analog precoder (combiner) shared by all the subcarriers [41]. Digital precoding precedes inverse fast fourier transform (IFFT), which is followed by analog precoding at the transmitter side. On the other hand, analog combining is succeeded by fast fourier transform (FFT) followed by digital combining at the receiver side. We consider that $S_c$ subcarriers are used in MIMO-OFDM transmission. The $m$th subcarrier for the RIS-receiver link [42] is

$$\mathbf{H}_{\mathrm{R}}[m] = \sqrt{\frac{N_I N_r}{L_R}}\sum_{\ell=1}^{L_R}\beta_\ell \mathbf{a}_R(\phi_\ell^R)\mathbf{a}_{RIS}(\phi_\ell^{RIS,t}, \theta_\ell^{RIS,t})^{H} e^{-j\frac{2\pi}{S_c}(\ell-1)m}, \qquad m = 0, \ldots, S_c - 1, \tag{21}$$

where $L_R$ represents the number of delay taps in time-domain RIS-receiver channel impulse response. We consider that the signal traveling through each of the paths in the channel experiences distinct delay, so we can think of each of the taps representing a separate path in the link [43]. The subcarriers for the transmitter-RIS link, denoted as $\left\{\mathbf{H}_{\mathrm{T}}[m]\right\}_{m=0}^{S_c-1}$, can be obtained in a similar manner. The effective $m$th subcarrier for the transmitter–receiver link is given by [27]

$$\mathbf{H}[m] = \mathbf{H}_{\mathrm{R}}[m]\boldsymbol{\Phi}\mathbf{H}_{\mathrm{T}}[m], \qquad m = 0, \ldots, S_c - 1. \tag{22}$$

We suggest referring to [27] for more details. RIS, devoid of RF chains, is only capable of *frequency-flat* passive beamforming [27]. Thus, the RIS reflection coefficients, unlike precoder/combiner, should be designed to serve all the subcarriers in the wideband MIMO-OFDM. Following the developments made for narrowband channel, the MSE for wideband MIMO-OFDM can be written as the sum of MSEs for all subcarriers,

$$\begin{aligned} \mathrm{MSE} = \sum_{m=0}^{S_c-1} \mathbf{Tr}\big[&\mathbf{I} - \mathbf{W}_{\mathrm{FD}}[m]^{H}\mathbf{H}_{\mathrm{R}}[m]\boldsymbol{\Phi}\mathbf{H}_{\mathrm{T}}[m]\mathbf{F}_{\mathrm{FD}}[m] \\ &- \mathbf{F}_{\mathrm{FD}}[m]^{H}\mathbf{H}_{\mathrm{T}}[m]^{H}\boldsymbol{\Phi}^{H}\mathbf{H}_{\mathrm{R}}[m]^{H}\mathbf{W}_{\mathrm{FD}}[m] \end{aligned}$$

$$+\mathbf{W}_{\mathrm{FD}}[m]^H\mathbf{H}_{\mathrm{R}}[m]\boldsymbol{\Phi}\mathbf{H}_{\mathrm{T}}[m]\mathbf{F}_{\mathrm{FD}}[m]\mathbf{F}_{\mathrm{FD}}[m]^H \mathbf{H}_{\mathrm{T}}[m]^H\boldsymbol{\Phi}^H\mathbf{H}_{\mathrm{R}}[m]^H\mathbf{W}_{\mathrm{FD}}[m]\big]. \tag{23}$$

Similar to the case in narrowband channel, it can be simplified as

$$\mathrm{MSE} = \sum_{m=0}^{S_c-1} \boldsymbol{\phi}\mathbf{C}[m]\boldsymbol{\phi}^H - \boldsymbol{\phi}\mathbf{t}[m] - \mathbf{t}^H[m]\boldsymbol{\phi}^H + \left(S_cN_s + \sigma_n^2 w[m] + u[m]\right), \tag{24}$$

where

$$\mathbf{t}[m] \triangleq \mathbf{diag}\left(\mathbf{H}_{\mathrm{T}}[m]\mathbf{F}_{\mathrm{FD}}[m]\mathbf{W}_{\mathrm{FD}}^H[m]\mathbf{H}_{\mathrm{R}}[m]\right), \tag{25a}$$

$$\mathbf{C}[m] \triangleq \left(\mathbf{H}_{\mathrm{T}}[m]\mathbf{F}_{\mathrm{FD}}[m]\mathbf{F}_{\mathrm{FD}}^H[m]\mathbf{H}_{\mathrm{T}}^H[m]\right)\odot \left(\mathbf{H}_{\mathrm{R}}^H[m]\mathbf{W}_{\mathrm{FD}}[m]\mathbf{W}_{\mathrm{FD}}^H[m]\mathbf{H}_{\mathrm{R}}[m]\right)^T, \tag{25b}$$

$$w[m] \triangleq \mathbf{Tr}\left[\mathbf{W}_{\mathrm{FD}}[m]^H\mathbf{W}_{\mathrm{FD}}[m]\right] \tag{25c}$$

$$u[m] \triangleq \mathbf{Tr}\big[\mathbf{W}_{\mathrm{FD}}[m]^H\mathbf{H}_{\mathrm{D}}[m]\mathbf{F}_{\mathrm{FD}}[m]\mathbf{F}_{\mathrm{FD}}[m]^H \mathbf{H}_{\mathrm{D}}[m]^H\mathbf{W}_{\mathrm{FD}}[m] - \mathbf{W}_{\mathrm{FD}}[m]^H\mathbf{H}_{\mathrm{D}}[m]\mathbf{F}_{\mathrm{FD}}[m] -\mathbf{F}_{\mathrm{FD}}[m]^H\mathbf{H}_{\mathrm{D}}[m]^H\mathbf{W}_{\mathrm{FD}}[m]\big]. \tag{25d}$$

Thus, passive beamforming problem can be written as

$$\boldsymbol{\phi}^\star = \arg\min_{\boldsymbol{\phi}} \quad \boldsymbol{\phi}\sum_{m=0}^{S_c-1}\mathbf{C}[m]\boldsymbol{\phi}^H - \boldsymbol{\phi}\sum_{m=0}^{S_c-1}\mathbf{t}[m] - \sum_{m=0}^{S_c-1}\mathbf{t}[m]^H\boldsymbol{\phi}^H + \left(S_cN_s + \sum_{m=0}^{S_c-1}\sigma_n^2 w[m] + u[m]\right) \quad \text{s.t.} \quad |\boldsymbol{\phi}_i| = 1, \quad \forall i = 1,\dots,N_I. \tag{26}$$

The passive beamforming problem for wideband channel is similar to the problem in narrowband channel (8), and can be solved by similar iterative method as in narrowband scenario. Using the results from narrowband case, $\mathbf{W}_{\mathrm{FD}}[m]$ and $\mathbf{F}_{\mathrm{FD}}[m]$ are calculated during each iteration as

$$\mathbf{W}_{\mathrm{FD}}[m] = \left(\mathbf{H}[m]\mathbf{F}_{\mathrm{FD}}[m]\mathbf{F}_{\mathrm{FD}}[m]^H\mathbf{H}[m]^H + \sigma_n^2\mathbf{I}_{N_r}\right)^{-1} \mathbf{H}[m]\mathbf{F}_{\mathrm{FD}}[m], \quad \forall m = 0,1,\dots,S_c-1, \tag{27}$$

$$\mathbf{F}_{\mathrm{FD}}[m] = \mathbf{V}[m]_{:,1:N_s}\boldsymbol{\Gamma}[\mathbf{m}], \forall m = 0,1,\dots,S_c-1, \tag{28}$$

where $\mathbf{V}[m]_{:,1:N_s}$ is the matrix containing the leading $N_s$ singular values of $\mathbf{H}[m]$, and $\boldsymbol{\Gamma}[\mathbf{m}]$ is the power loading matrix for the $m$th subcarrier. $\boldsymbol{\phi}$ is calculated as

$$\boldsymbol{\phi} = \exp\left(j\angle\left(\left(\sum_{m=0}^{S_c-1}\mathbf{t}[m]^H\right)\left(\sum_{m=0}^{S_c-1}\mathbf{C}[m] + \mu\mathbf{I}\right)^{-1}\right)\right), \tag{29}$$

where

$$\mu = \frac{1}{N_I}\left(S_cN_s + \sum_{m=0}^{S_c-1}\sigma_n^2 w[m] + u[m]\right). \tag{30}$$

### 5.2 | Hybrid precoding for wideband channel

The hybrid precoding problem for mmWave MIMO-OFDM can be written as [44, 45]

$$\min_{\mathbf{F}_{\mathrm{R}},\mathbf{F}_{\mathrm{FD}}[m]} \quad \sum_{m=0}^{S_c-1}\left\|\mathbf{F}_{\mathrm{FD}}[m] - \mathbf{F}_{\mathrm{R}}\mathbf{F}_{\mathrm{D}}[m]\right\|_F^2 \quad \text{s.t.} \quad \left\|\mathbf{F}_{\mathrm{R}}\mathbf{F}_{\mathrm{D}}[m]\right\|_F^2 = N_s, \quad \left|\mathbf{F}_{\mathrm{R}_{i,j}}\right| = 1, \ \forall i,j, \tag{31}$$

where $\mathbf{F}_{\mathrm{FD}}[m]$ is the fully digital precoder for the $m$th subcarrier and the $\mathbf{F}_{\mathrm{D}}[m]$ is the digital precoder of the hybrid precoder for the $m$th subcarrier. The analog precoding subproblem for the wideband channel can be written in terms of $\bar{\mathbf{F}}_{\mathrm{R}}$ similar to the narrowband case [36].

$$\max_{\bar{\mathbf{F}}_{\mathrm{R}}} \quad \mathbf{Tr}\left[\bar{\mathbf{F}}_{\mathrm{R}}^H\left(\sum_{m=0}^{S_c-1}\mathbf{F}_{\mathrm{FD}}[m]\mathbf{F}_{\mathrm{FD}}[m]^H\right)\bar{\mathbf{F}}_{\mathrm{R}}\right] \quad \text{s.t.} \quad \text{(19b) and (19c).} \tag{32}$$

We can solve for $\mathbf{F}_{\mathrm{R}} = \sqrt{N_t}\bar{\mathbf{F}}_{\mathrm{R}}$ by solving (30) using Algorithm 2, where $\mathbf{A}^k$ is computed during each $k$th iteration as $\mathbf{A}^k = \bar{\mathbf{F}}_{\mathrm{R}}^{(k-1)^H}\left(\sum_{m=0}^{S_c-1}\mathbf{F}_{\mathrm{FD}}[m]\mathbf{F}_{\mathrm{FD}}[m]^H\right)$. After determining $\mathbf{F}_{\mathrm{R}}$, the digital precoder for $m$th subcarrier can be determined as $\mathbf{F}_{\mathrm{D}}[m] = \mathbf{F}_{\mathrm{R}}^\dagger\mathbf{F}_{\mathrm{FD}}[m]$.

## 6 | COMPLEXITY ANALYSIS OF THE PROPOSED METHOD

In this section, the computational complexity of the proposed method is evaluated. The complexity of the proposed method is calculated for narrowband channel, followed by the wideband channel.

### 6.1 | Complexity analysis of the proposed method in narrowband channel

The complexity of computing the RIS phase-shift matrix and the hybrid precoder are computed separately.

(i) *Computation of RIS phase-shift matrix* $\boldsymbol{\Phi}$:
- *Computation of* $\mathbf{F}_{\mathrm{FD}}$: The evaluation of SVD of the $N_r \times N_t$ channel matrix governs the complexity, entailing a complexity of $\mathcal{O}(N_t^2N_r)$.

- *Computation of* $\mathbf{W}_{\text{FD}}$: The major complexity in computation comes from inverse operation of an $N_r \times N_r$ matrix which is $\mathcal{O}\left(N_r^3\right)$.
- *Computation of* $\boldsymbol{\phi}$: The inverse of an $N_I \times N_I$ matrix that involves a complexity of $\mathcal{O}\left(N_I^3\right)$ contributes mainly to the complexity.
- *Computation of channel matrix* $\mathbf{H}$: The computation of $\mathbf{H}$ requires a multiplication between the $N_r \times N_I$ matrix $\mathbf{H}_{\text{R}}$, the $N_I \times N_I$ matrix $\boldsymbol{\Phi}$ and the $N_I \times N_t$ matrix $\mathbf{H}_{\text{T}}$ which has a complexity of $\mathcal{O}\left(N_r N_I^2 + N_r N_I N_t\right)$.

Each of these operations are repeated $N_{it}^{\text{PP}}$ times, so the total complexity of computing is $N_{it}^{\text{PP}}\mathcal{O}({N_I}^3 + N_r^3 + N_t^2 N_r + N_r N_I^2 + N_r N_I N_t)$.

(ii) *Computation of hybrid precoder*: $\mathbf{F}_{\text{FD}}$ needs to be computed from $\mathbf{H}$ which entails a complexity of $\mathcal{O}(N_t^2 N_r + {N_r}^2 N_t)$. Computing $\mathbf{F}_{\text{FD}}\mathbf{F}_{\text{FD}}^H$ has a complexity of $\mathcal{O}(N_t^2 N_s)$. It can be deduced that the computation of analog part of the precoder from $\mathbf{F}_{\text{FD}}$ comes with a complexity of $\mathcal{O}(N_t^2 N_r + {N_r}^2 N_t + N_t^2 N_s) + N_{iter}^{HP}\mathcal{O}(N_t^2 M_t + 2N_t M_t^2)$, where $N_{iter}^{HP}$ is the number of iterations performed [40]. The majority of complexity in the computation of digital precoder comes from pseudo inverse operation which is $\mathcal{O}(N_t^2 M_t)$.

## 6.2 | Complexity analysis of the proposed method in wideband channel

The complexity can be easily computed from the complexity of the narrowband counterpart.

(i) *Computation of RIS phase-shift matrix* $\boldsymbol{\Phi}$: The computation of $\mathbf{F}_{\text{FD}}[m]$, $\mathbf{W}_{\text{FD}}[m]$ and $\mathbf{H}[m]$ should be performed for $S_c$ subcarriers. Thus, the complexity of computing phase-shift matrix $\boldsymbol{\Phi}$ is $N_{it}^{\text{PP}}\mathcal{O}(N_I^3 + S_c(N_r^3 + N_t^2 N_r + N_r N_I^2 + N_r N_I N_t))$.

(ii) *Computation of hybrid precoder*: The complexity in computing analog precoder is $S_c\mathcal{O}(N_t^2 N_r + {N_r}^2 N_t + N_t^2 N_s) + N_{iter}^{HP}\mathcal{O}(N_t^2 M_t + 2N_t M_t^2)$. The digital precoder requires a complexity of $S_c\mathcal{O}(N_t^2 M_t)$.

Tables 1 and 2 summarize the complexities of the proposed passive beamforming algorithm along with various existing passive beamforming methods in narrowband channel and wideband channel, respectively. $N_{it}^{\text{TSVD}}$, $N_{it}^{\text{AO}}$, $N_{it}^{\text{SPGM}}$ and $N_{it}^{\text{TSVD-MO}}$ in Tables 1 and 2 represent the number of iterations required for passive beamforming algorithms in [9, 21, 27] and [30], respectively. On the other hand, $N_{it_{in}}^{\text{WMMSE}}$ ($N_{it_o}^{\text{WMMSE}}$) is the number of inner (outer) iterations needed for the algorithm in [19]. The complexities of [19, 27] and [21] have been sourced from [9].

**TABLE 1** Comparison of computational complexity of different passive beamforming algorithms in narrowband channel.

| Algorithm | Complexity |
|---|---|
| Proposed MMSE-PP | $N_{it}^{\text{PP}}\mathcal{O}\left({N_I}^3 + N_r^3 + N_t^2 N_r + N_r N_I^2 + N_r N_I N_t\right)$ |
| T-SVD [9] | $\mathcal{O}\left(N_{it}^{\text{TSVD}} N_I + N_t N_r^2\right)$ |
| AO [27] | $\mathcal{O}\left(N_r N_t\left(N_I + N_r\right)N_{it}^{\text{AO}} + \left(3N_r^3 + 2N_r^2 N_t + N_t^2\right)N_I\right)$ |
| SPGM [21] | $\mathcal{O}\left(N_{it}^{\text{SPGM}} N_I^3\right)$ |
| WMMSE [19] | $N_{it_o}^{\text{WMMSE}}\mathcal{O}\left(N_r^3 + N_s^3 + N_t^3 + N_I^3 + N_{it_{in}}^{\text{WMMSE}} N_I^2\right)$ |
| AMEV [29] | $\mathcal{O}\left(N_t N_r N_I\right)$ |
| TSVD-MO [30] | $\mathcal{O}\left(N_{it}^{\text{TSVD-MO}} N_I + N_t N_r^2\right)$ |

**TABLE 2** Comparison of computational complexity of different passive beamforming algorithms in wideband channel.

| Algorithm | Complexity |
|---|---|
| Proposed MMSE-PP | $N_{it}^{\text{PP}}\mathcal{O}\left(N_I^3 + S_c\left(N_r^3 + N_t^2 N_r + N_r N_I^2 + N_r N_I N_t\right)\right)$ |
| SPGM [21] | $\mathcal{O}\left(N_{it}^{\text{SPGM}} N_I^3\right)$ |
| AMEV [29] | $\mathcal{O}\left(S_c N_t N_r N_I\right)$ |
| TSVD-MO [30] | $\mathcal{O}\left(N_{it}^{\text{TSVD-MO}} N_I + S_c N_t N_r^2\right)$ |

## 7 | PERFORMANCE ANALYSIS

A point-to-point mmWave MIMO is considered in which BS, RIS and UE are placed at $(x_B, 0, z_B)$, $(0, y_R, z_R)$ and $(x_{Rx}, y_{Rx}, z_{Rx})$, respectively, where $x_B = 2$ m, $z_B = 10$ m, $y_R = 148$ m, $z_R = 10$ m, $x_{Rx} = 5$ m, $y_{Rx} = 150$ m, $z_{Rx} = 1.8$ m. We assume that no direct link exists between the BS and the receiver. It is assumed that the BS and the UE are both equipped with ULA having $N_t = 64$ and $N_r = 16$ antennas, respectively, whereas the RIS utilizes square UPA with $N_I = N_I^y \times N_I^z$ elements. The number of RF chains at the BS and the UE are taken to be equal to $N_s$. The values of $N_s$ and $N_I$ are taken as 4 and 100, respectively, unless they are varying parameters. All the antenna elements are separated by a distance of half wavelength. The noise power $\sigma_n^2 = 90$ dBm. The number of paths in the BS-RIS link and RIS-UE link is chosen to be $L = 7$ including the LOS path. The complex gain of the LOS path is $\alpha_1(\beta_1) \sim \mathcal{CN}(0, 10^{-\kappa})$, where $\kappa$ indicates the path loss given by [46]

$$\kappa = a + 10b\, log_{10}(\tilde{d}) + \xi, \tag{33}$$

in which $\xi \sim \mathcal{N}(0, \sigma_\xi^2)$, $\tilde{d} = \tilde{d}_{Tx-RIS}$ or $\tilde{d} = \tilde{d}_{RIS-Rx}$ denotes the distance between the transmitter and the RIS, or the distance between the RIS and receiver, respectively. The complex gain of NLOS path is $\alpha_i(\beta_i) \sim \mathcal{CN}(0, 10^{-(\kappa+\mu_R)})$ where $\mu_R$ is the Rician factor. The values $a = 61.4$, $b = 2$, and $\sigma_\xi = 5.8$ dB are taken based on the results from real-world measurements [46], while the value of $\mu_R$ is taken as 10. We take the number of subcarriers $S_c = 128$ in wideband channel. The simulation parameters are listed in Table 3.

The performance of the proposed method is compared with sum-path gain maximization based passive beamforming (SPGM) [21], asymptotic maximization of eigenvalue based passive beamforming (AMEV) [29], and the high-performance

**TABLE 3** Parameters for simulations.

| Parameters | Values |
|---|---|
| $N_t$ | 64 ULA |
| $N_r$ | 16 ULA |
| $N_I$ | $10 \times 10$ UPA |
| $L$ | 7 |
| $N_s$ | 4 |
| BS location: $(x_B, y_B, z_B)$ | (2 m, 0 m, 10 m) |
| RIS location: $(x_R, y_R, z_R)$ | (0 m, 148 m, 10 m) |
| Receiver location: $(x_{Rx}, y_{Rx}, z_{Rx})$ | (5 m, 150 m, 1.8 m) |
| $\sigma_n^2$ | 90 dBm |
| LOS path gain: $\alpha_1(\beta_1)$ | $\sim \mathcal{CN}(0, 10^{-\kappa})$ |
| NLOS path gain: $\alpha_i(\beta_i),\ i = 2, \ldots, L$ | $\sim \mathcal{CN}(0, 10^{-(\kappa+\mu)})$ |
| $\kappa$ | $a + 10b\ log_{10}(\tilde{d}) + \xi$ |
| $a$ | 61.4 |
| $b$ | 2 |
| $\mu_R$ | 10 |
| $\xi$ | $\sim \mathcal{N}(0, \sigma_\xi^2)$ |
| $\sigma_\xi$ | 5.8 dB |
| $\tilde{d}_{Tx-RIS}$ | $\sqrt{(x_R - x_B)^2 + (y_R - y_B)^2 + (z_R - z_B)^2}$ |
| $\tilde{d}_{RIS-Rx}$ | $\sqrt{(x_{Rx} - x_R)^2 + (y_{Rx} - y_R)^2 + (z_{Rx} - z_R)^2}$ |
| $S_c$ | 128 *(for wideband)* |

methods like alternating optimization based passive beamforming (AO) [27], truncated SVD based passive beamforming (T-SVD) [9] and truncated SVD based passive beamforming for MIMO-OFDM (TSVD-MO) [30] in narrowband channel, and with the SPGM, AMEV and TSVD-MO in wideband scenario. It should be noted that T-SVD and TSVD-MO algorithms are exactly the same in narrowband channel when there is no direct channel between the transmitter and the receiver. In the figures, *Proposed Hybrid* refers to the proposed RIS design method with hybrid precoder, whereas *Proposed Fully Digital* alludes to the proposed RIS design method with fully digital precoder. All other compared methods use fully digital precoder except hybrid T-SVD [9].

## 7.1 | Convergence behavior

We plot the convergence behavior of the proposed method in narrowband and wideband channels in Figures 2 and 3, respectively, under different parameters. It can be seen that the proposed method converges after few iterations in both narrowband and wideband channels, confirming the good convergence behavior of the proposed method.

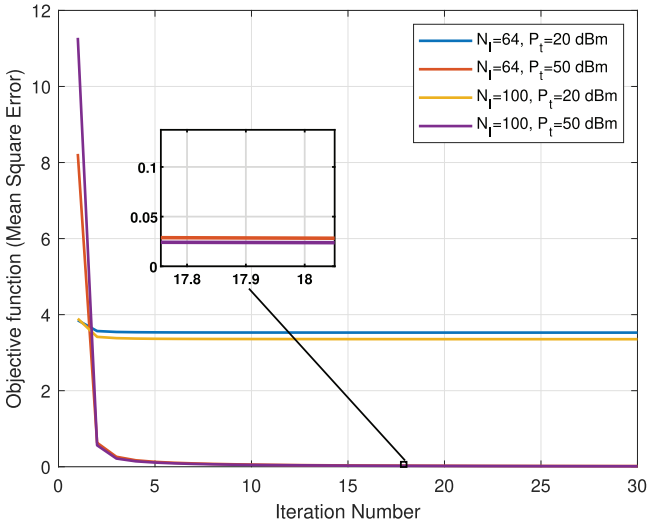


**FIGURE 2** Convergence behavior of the proposed method in narrowband channel, $N_s = 4$.

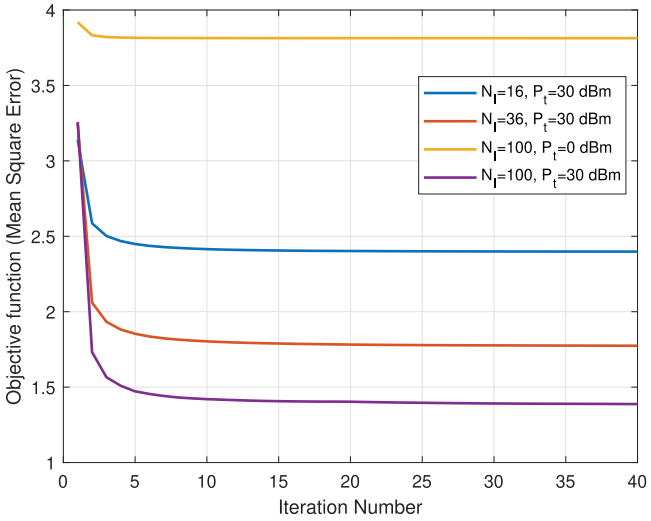


**FIGURE 3** Convergence behavior of the proposed method in wideband channel, $N_s = 4$.

## 7.2 | Narrowband channel

In Figure 4, the spectral efficiency is plotted as a function of transmit power. The figure shows the performances of the proposed method and T-SVD with both the fully digital precoder and the hybrid precoder. The figure clearly shows that the proposed method performs better than T-SVD / TSVD-MO by a good margin, and the performance gaps with SPGM and AMEV are huge. The proposed method performs marginally better than AO. It can be seen that performance similar to the fully digital precoder can be achieved with the hybrid precoder. When the spectral performance in Figure 5 is observed as $N_I$ is varied, it can be seen that the spectral efficiency increases with $N_I$ for all methods. The proposed method is clearly ahead of SPGM, AMEV and T-SVD/TSVD-MO in spectral

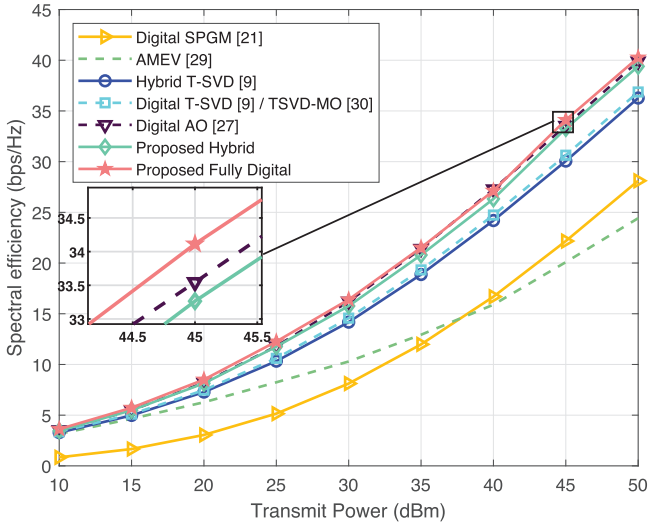


**FIGURE 4** Spectral efficiency versus transmit power, $N_I = 100$, $M_t = N_s = 4$.

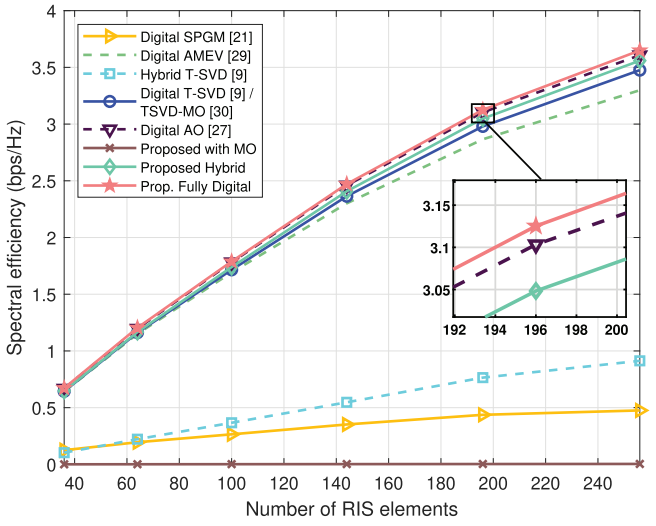


**FIGURE 6** Spectral efficiency versus the number of RIS elements, $P_t = 0$ dBm, $M_t = N_s = 2$.

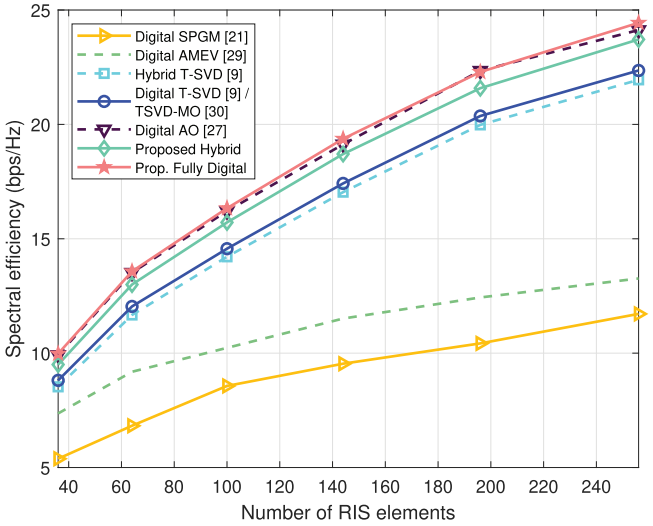


**FIGURE 5** Spectral efficiency versus the number of RIS elements, $P_t = 30$ dBm, $M_t = N_s = 4$.

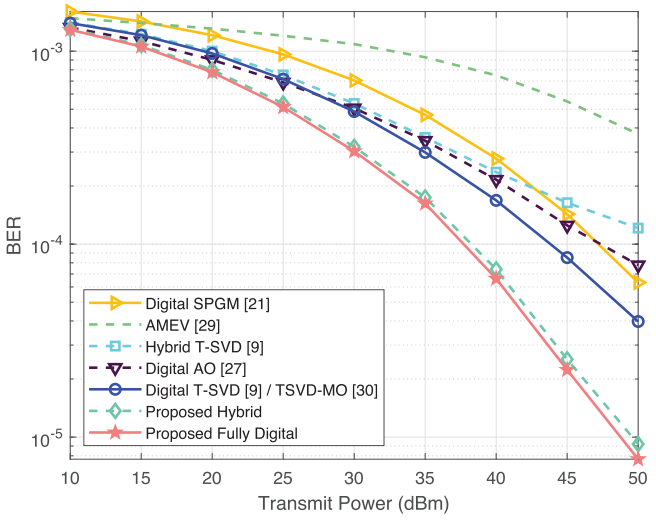


**FIGURE 7** Bit error rate versus transmit power, $N_I = 100$, $M_t = N_s = 4$.

performance. This proves that the spectral performance in the proposed method is consistently very good for wide range of number of RIS elements. The spectral performance of the proposed method is slightly better than the AO. Another observation that can be made is that the difference in performances of the proposed method with the fully digital precoder and the hybrid precoder is not significant. This proves that the hybrid precoder is able to emulate the performance of fully digital precoder successfully even with the minimum number of RF chains. It should be noted that the minimum number of RF chains required to multiplex $N_s$ data streams is $N_s$. Furthermore, we also show the spectral efficiency performance at lower power in Figure 6. The proposed method (both the fully digital and hybrid one) deliver excellent spectral performance even at low power. AMEV, otherwise a bad performer, shows good performance at low power. However, hybrid T-SVD falls behind in its spectral performance at low power.

The BER performance as a function of the transmit power in Figure 7 and the BER performance as a function of the number of RIS elements in Figure 8 (high transmit power regime) and Figure 9 (low transmit power regime) clearly show the superiority of the proposed method over all other methods. The existing state-of-the-art passive beamforming methods like T-SVD, TSVD-MO and AO with very good spectral performances, leave a lot to be desired when we look at their bit error rate (BER) performances. Hybrid T-SVD performs pretty badly in low power regime. Actually, the BER performance of the proposed RIS design method with hybrid precoder (having minimum number of RF chains) outperforms the existing superior methods with fully digital precoder by a good margin. The superior BER performance proves that the proposed method which

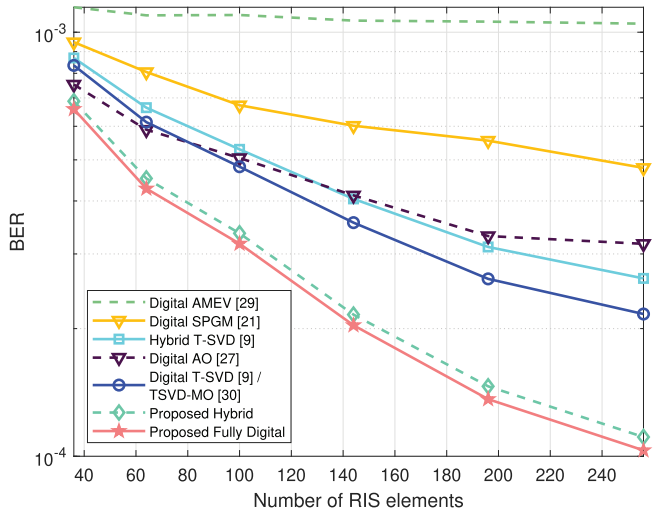


**FIGURE 8** Bit error rate versus the number of RIS elements, $P_t = 30$ dBm, $M_t = N_s = 4$.

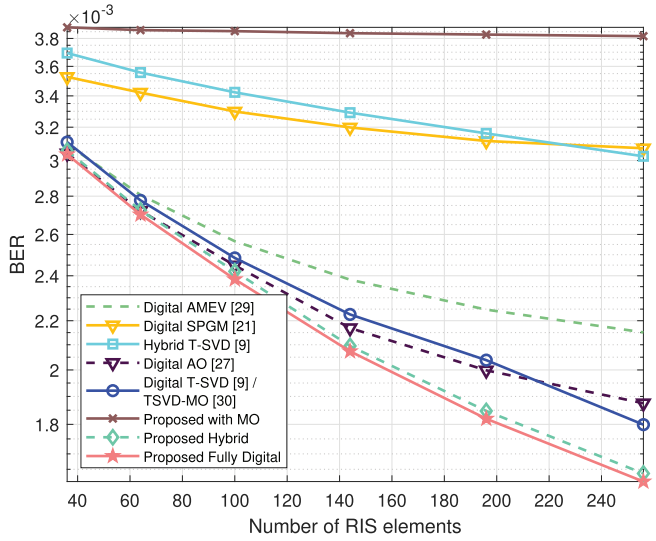


**FIGURE 9** Bit error rate versus the number of RIS elements, $P_t = 0$ dBm, $M_t = N_s = 2$.

designs $\mathbf{\Phi}$ by minimizing the MSE between the transmit signal and the received signal is successful in achieving low MSE.

In Figure 10, the truncated condition number of the channel between the BS and the UE is plotted. The condition number of a channel is defined as

$$\zeta = \frac{\lambda_{max}}{\lambda_{min}}, \tag{34}$$

where $\lambda_{max}$ and $\lambda_{min}$ are the maximum and minimum singular values of the channel, respectively. Since we transmit only $N_s$ streams over $\mathbf{H}$, we consider truncated condition number of the channel. If $\lambda_1, \ldots, \lambda_{N_s}$ are the $N_s$ largest singular values of the channel arranged in descending order, the truncated condition

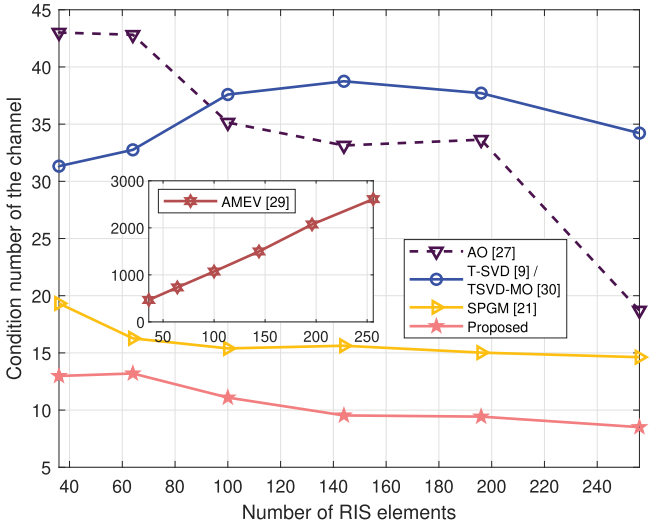


**FIGURE 10** Condition number of the channel versus the number of RIS elements, $P_t = 50$ dBm, $N_s = 4$.

number of the channel is defined as [9]

$$\zeta_{tr} = \frac{\lambda_1}{\lambda_{N_s}}. \tag{35}$$

The truncated condition number in case of the AO-method is the largest at lower values of $N_I$ but gets smaller with increasing $N_I$. It is still larger than those of SPGM and the proposed method even at higher $N_I$. The condition number of the channel with the proposed method has the lowest values, varying between 13 at $N_I = 36$ and 8 at $N_I = 256$. The condition number of the channel in case of the proposed method exhibits the least erratic plot across the wide range of $N_I$ values. The channel with singular values that are spread less, or lower condition number have large capacity at high SNR, in general. The condition number closer to 1 is desirable as it makes the channel well-conditioned [47]. Thus, Figure 10 attests that the proposed method produces more well-conditioned channel in comparison to other methods.

To numerically compare the computational complexities of the various methods, we plot the average runtimes as a function of $N_I$ in Figure 11. All the algorithms are executed in MATLAB2023a on a personal computer with Intel Core i7 2.8 GHz processor and 16 GB RAM. It can be observed that the average runtime for the AO-method is the highest and that for AMEV is the lowest. However, the lower complexity of AMEV comes at the price of extremely poor spectral and BER performances. The average runtimes of the SPGM and the proposed method are also on the lower side. The average runtime for SPGM are smaller compared to the proposed method at lower values of $N_I$ but as $N_I$ increases the runtime for the proposed method gets lower than SPGM. Thus, we can say the proposed method is computationally-efficient, whereas the AO-method is computationally grueling.

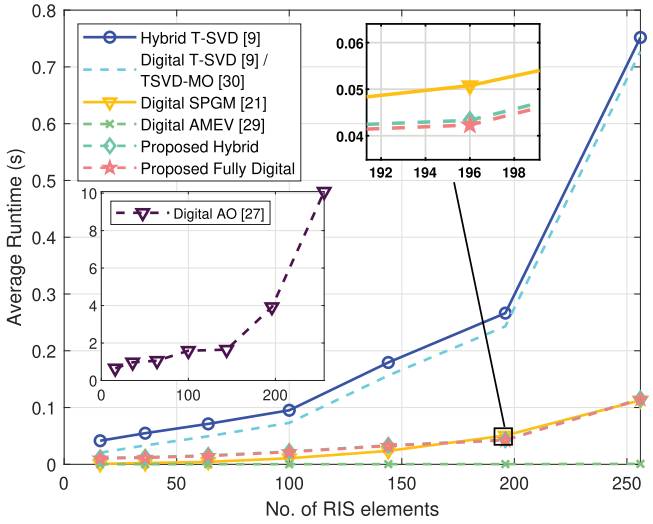


**FIGURE 11** Average run time versus the number of RIS elements, $M_t = N_s = 4$.

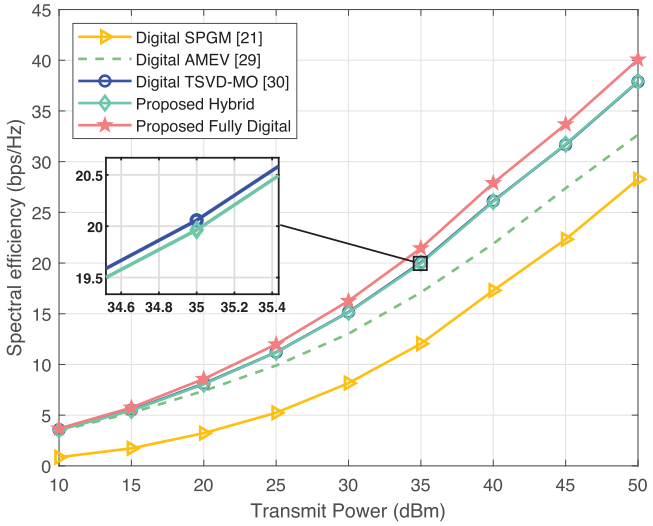


**FIGURE 13** Spectral efficiency versus transmit power, $N_I = 100$, $M_t = N_s = 4$.

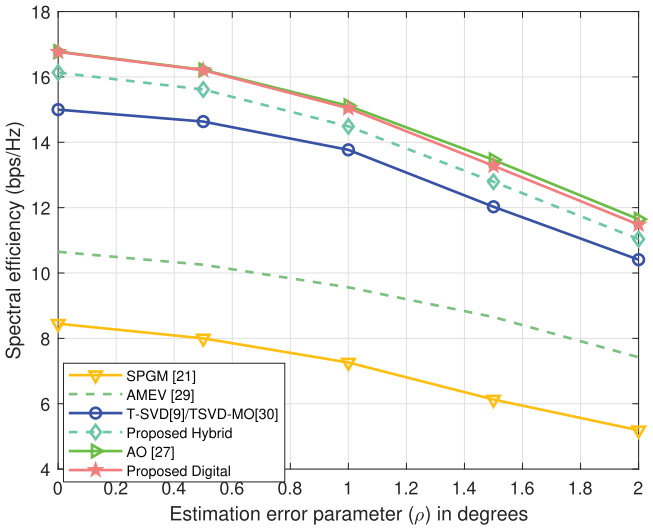


**FIGURE 12** Estimation error rate versus estimation error parameter $\delta$, $N_I = 100$, $M_t = N_s = 4$, $P_t = 30$ dBm.

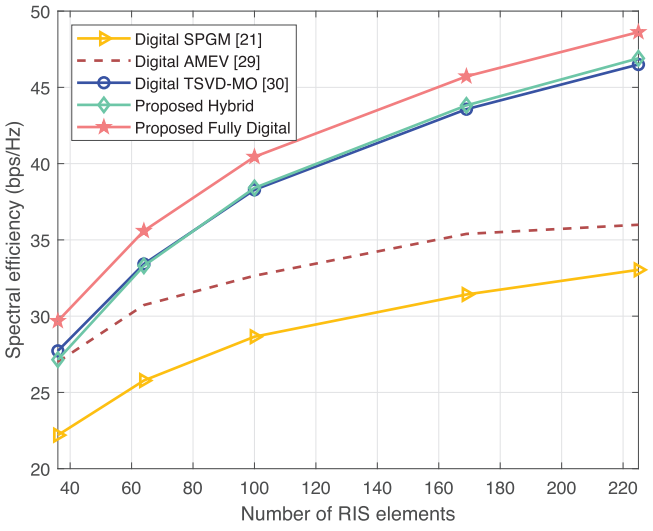


**FIGURE 14** Spectral efficiency versus the number of RIS elements, $P_t = 50$ dBm, $M_t = N_s = 4$.

## 7.3 | Effect of channel estimation error

We have assumed the availability of perfect channel state information (CSI). In this section, we investigate how the proposed passive beamforming method performs when the CSI available is imperfect. To this end, we assume that there is error in the estimation of AoDs/AoAs and see how the spectral efficiency performance of the proposed solution compares with the performances of the existing passive beamforming algorithms. If $\psi$ represents the true value of AoD/AoA and $\hat{\psi}$ the estimated value, estimation error in AoD/AoA is given by $\delta = \psi - \hat{\psi}$. Similar to [9], the errors in estimation of AoD/AoA are modeled as independent and identically distributed (i.i.d.) random variables having the same uniform probability distribution as

$$f(\delta) = \begin{cases} \frac{1}{2\rho}, & \text{if } -\rho \le \delta \le \rho \\ 0, & \text{otherwise} \end{cases}. \tag{36}$$

The spectral efficiency of the proposed method in narrowband channel is compared against the existing methods as a function of estimation error parameter $\rho$ in Figure 12. The Figure 12 reveals that the proposed method has similar degradation in performance with the increase in estimation error as the AO [27], T-SVD [9], TSVD-MO [30] and AMEV [29] whereas SPGM [21] suffers the worst performance loss. Thus, it can be said that the proposed method offers considerable robustness against the channel estimation errors which is comparable to the existing high-performing methods.

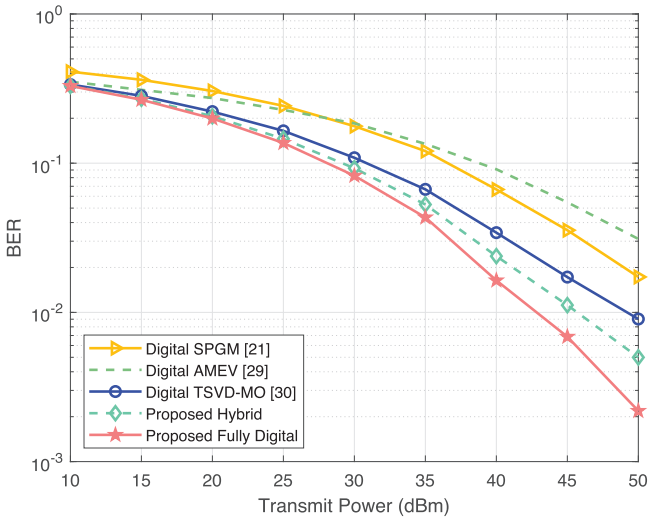


**FIGURE 15** Bit error rate versus transmit power, $N_I = 100$, $M_t = N_s = 4$.

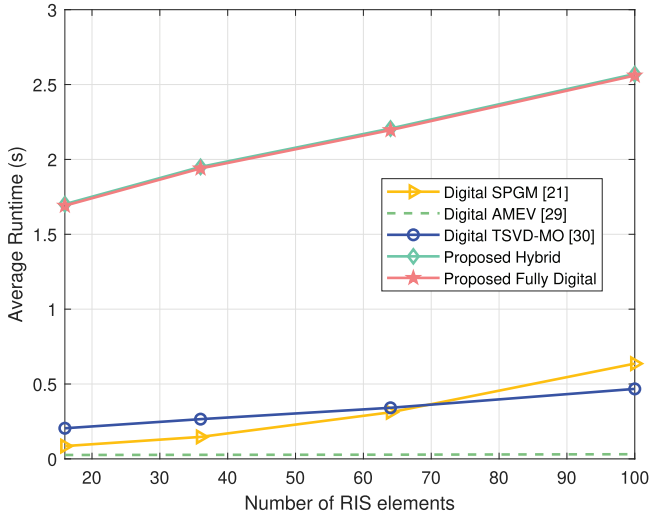


**FIGURE 16** Average runtime versus the number of RIS elements, $P_t = 50$ dBm, $M_t = N_s = 4$.

## 7.4 | Wideband channel

The spectral efficiency is plotted as a function of transmit power and number of RIS elements, respectively, in Figures 13 and 14, whereas BER performance is plotted as a function of transmit power in Figure 15. In Figure 16, average runtime of various algorithms is plotted against the number of RIS elements.

The proposed method exhibits superior performance in wideband scenario, similar to its performance in narrowband channel. The spectral and BER performances in Figures 13 and 15, respectively, depict that the proposed method is clearly performing very well and clearly ahead of the SPGM, AMEV and TSVD-MO. The spectral efficiency plot against the number of RIS elements in Figure 14 shows that the performance of the proposed method is considerably better than that of TSVD-MO. The spectral performance of the proposed method gets better than the SPGM/AMEV as the number of RIS elements grows. It establishes the proposed method's ability to design the RIS phase shift coefficients in such a way that the channel is programmed to extract better performance. Although the average runtime of the proposed method is higher than those of the compared algorithms, it still is on the lower side.

To provide a summary, we list various passive beamforming methods with their attributes and compare the proposed method against each of them in Table 4. The second column of table lists the features of the respective beamforming method

**TABLE 4** Comparison of proposed method with various passive beamforming algorithms.

| Algorithm | Features | Proposed method (in comparison) |
|---|---|---|
| T-SVD [9] | - Obj: Maximize spectral efficiency<br>- Good spectral performance<br>- Good BER performance<br>- Moderate complexity in narrowband<br>- Does not work in wideband | - Obj: Minimize MSE between Tx and Rx signals<br>- Better spectral performance<br>- Much better BER performance<br>- Lower complexity in narrowband<br>- Works in wideband |
| TSVD-MO [30] | - Obj: Maximize spectral efficiency<br>- Very good spectral performance<br>- Good BER performance in narrowband, poor in wideband<br>- Moderate complexity in narrowband, low in wideband | - Obj: Minimize MSE between Tx and Rx signals<br>- Better spectral performance<br>- Much better BER performance in both narrowband & wideband<br>- Lower complexity in narrowband, higher in wideband |
| SPGM [21] | - Obj: Maximize channel power<br>- Poor spectral performance<br>- Poor BER performance<br>- Low complexity in both narrowband and wideband | - Obj: Minimize MSE between Tx & and Rx signals<br>- Much better spectral performance<br>- Much better BER performance<br>- Similar complexity in narrowband, higher in wideband |
| AMEV [29] | - Obj: Maximize dominant singular value of RIS-UE channel<br>- Very poor spectral performance<br>- Very poor BER performance<br>- Extremely low complexity in both narrowband and wideband | - Obj: Minimize MSE between Tx and Rx signals<br>- Much better spectral performance<br>- Much better BER performance<br>- Higher complexity in both narrowband and wideband |
| AO [27] | - Obj: Maximize capacity<br>- Excellent spectral performance<br>- Good BER performance<br>- Very high complexity in narrowband<br>- Does not work in wideband | - Obj: Minimize MSE between Tx and Rx signals<br>- Similar spectral performance<br>- Much better BER performance<br>- Lower complexity in narrowband<br>- Works in wideband |

Obj = objective; Tx = transmit; Rx = receive.

and the third column compares the proposed method against each of the features of listed methods.

## 8 | CONCLUSION

An mmWave narrowband downlink MIMO is considered which is assisted by an RIS. The passive beamforming at the RIS, the fully digital precoding at the BS and the fully digital combining at the receiver are jointly designed. The RIS phase shift matrix is designed to minimize the MSE between the transmit signal and the estimate of received signal in an iterative fashion. The RIS passive beamforming vector is obtained by normalizing each element of the unconstrained solution vector of the equivalent MMSE passive beamforming problem. The hybrid precoder and combiner are constructed once the passive beamforming solution is obtained. The simulation results exhibit that the proposed method produces spectral performances and BER performances which are better than the existing solutions, including the best of state-of-the-art methods. The proposed method is extended for wideband MIMO-OFDM where it echoes its excellent narrowband performance. The proposed passive beamforming method achieves superior performance with only modest computational complexity. The reasons for the excellent performance of the proposed method are the choice of MSE as the objective function to determine passive beamforming and joint optimization. Provided a good algorithm is employed to minimize MSE, it is bound to give good results as the error between transmit signal and receive signal is reduced. Passive beamforming, in a way, is coupled with transmit precoding and receive combining as it forms a part of the equivalent channel. Thus, employing joint optimization of the precoding, combining and passive beamforming in the proposed method help in achieving overall good performance. The proposed passive beamforming algorithm proves to be effective at minimizing MSE and thus producing good spectral and BER performances, as attested by the simulation results. The involvement of a simple matrix inversion operation followed by phase extraction in the proposed algorithm, coupled with the convergence of joint optimization in few iterations help the proposed method achieve low complexity.

## AUTHOR CONTRIBUTIONS

**Prabhat Raj Gautam**: Conceptualization; formal analysis; investigation; methodology; software; validation; writing—original draft; writing—review and editing. **Li Zhang**: Supervision; writing—review and editing. **Pingzhi Fan**: Writing—review and editing.

## CONFLICT OF INTEREST STATEMENT

The authors declare no conflicts of interest.

## DATA AVAILABILITY STATEMENT

Data sharing is not applicable to this article as no new data were created or analyzed in this study.

## ORCID

*Prabhat Raj Gautam* https://orcid.org/0000-0001-9881-1394

## REFERENCES

1. Chin, W.H., Fan, Z., Haines, R.: Emerging technologies and research challenges for 5G wireless networks. IEEE Wireless Commun. 21(2), 106–112 (2014)
2. Swindlehurst, A.L., Ayanoglu, E., Heydari, P., Capolino, F.: Millimeter-wave massive MIMO: The next wireless revolution? IEEE Commun. Mag. 52, 56–62 (2014)
3. Rappaport, T.S., Murdock, J.N., Gutierrez, F.: State of the art in 60-ghz integrated circuits and systems for wireless communications. Proc. IEEE 99(8), 1390–1436 (2011)
4. Rangan, S., Rappaport, T.S., Erkip, E.: Millimeter-wave cellular wireless networks: Potentials and challenges. Proc. IEEE 102(3), 366–385 (2014)
5. Ghosh, A., Thomas, T.A., Cudak, M.C., Ratasuk, R., Moorut, P., Vook, F.W., Rappaport, T.S., MacCartney, G.R., Sun, S., Nie, S.: Millimeter-wave enhanced local area systems: A high-data-rate approach for future wireless networks. IEEE J. Sel. Areas Commun. 32(6), 1152–1163 (2014)
6. Wang, C.-X., Haider, F., Gao, X., You, X.-H., Yang, Y., Yuan, D., Aggoune, H.M., Haas, H., Fletcher, S., Hepsaydir, E.: Cellular architecture and key technologies for 5g wireless communication networks. IEEE Commun. Mag. 52(2), 122–130 (2014)
7. Bogale, T.E., Le, L.B.: Beamforming for multiuser massive MIMO systems: Digital versus hybrid analog-digital. In: 2014 IEEE Global Communications Conference, pp. 4066–4071. IEEE, Piscataway (2014)
8. ElMossallamy, M.A., Zhang, H., Song, L., Seddik, K.G., Han, Z., Li, G.Y.: Reconfigurable intelligent surfaces for wireless communications: Principles, challenges, and opportunities. IEEE Trans. Cogn. Commun. Network. 6(3), 990–1002 (2020)
9. Wang, P., Fang, J., Dai, L., Li, H.: Joint transceiver and large intelligent surface design for massive MIMO mmwave systems. IEEE Trans. Wireless Commun. 20(2), 1052–1064 (2021)
10. Wu, Q., Zhang, S., Zheng, B., You, C., Zhang, R.: Intelligent reflecting surface-aided wireless communications: A tutorial. IEEE Trans. Commun. 69(5), 3313–3351 (2021)
11. Björnson, E., Özdogan, Ö, Larsson, E.G.: Reconfigurable intelligent surfaces: Three myths and two critical questions. IEEE Commun. Mag. 58(12), 90–96 (2020)
12. Basar, E.: Transmission through large intelligent surfaces: A new frontier in wireless communications. In: 2019 European Conference on Networks and Communications (EuCNC), pp. 112–117. IEEE, Piscataway (2019)
13. Basar, E., Di Renzo, M., De Rosny, J., Debbah, M., Alouini, M.-S., Zhang, R.: Wireless communications through reconfigurable intelligent surfaces. IEEE Access 7, 116753–116773 (2019)
14. Liaskos, C., Nie, S., Tsioliaridou, A., Pitsillides, A., Ioannidis, S., Akyildiz, I.: A new wireless communication paradigm through software-controlled metasurfaces. IEEE Commun. Mag. 56(9), 162–169 (2018)
15. Renzo, M.D., Debbah, M., Phan-Huy, D.-T., Zappone, A., Alouini, M.-S., Yuen, C., Sciancalepore, V., Alexandropoulos, G.C., Hoydis, J., Gacanin, H., et al.: Smart radio environments empowered by reconfigurable AI meta-surfaces: An idea whose time has come. EURASIP J. Wirel. Commun. Network. 2019(1), 1–20 (2019)
16. Di Renzo, M., Ntontin, K., Song, J., Danufane, F.H., Qian, X., Lazarakis, F., De Rosny, J., Phan-Huy, D.-T., Simeone, O., Zhang, R., Debbah, M., Lerosey, G., Fink, M., Tretyakov, S., Shamai, S.: Reconfigurable intelligent surfaces vs. relaying: Differences, similarities, and performance comparison. IEEE Open J. Commun. Soc. 1, 798–807 (2020)
17. Di Renzo, M., Zappone, A., Debbah, M., Alouini, M.-S., Yuen, C., de Rosny, J., Tretyakov, S.: Smart radio environments empowered by reconfigurable intelligent surfaces: How it works, state of research, and the road ahead. IEEE J. Sel. Areas Commun. 38(11), 2450–2525 (2020)
18. Yuan, X., Zhang, Y.-J.A., Shi, Y., Yan, W., Liu, H.: Reconfigurable-intelligent-surface empowered wireless communications: Challenges and opportunities. IEEE Wireless Commun. 28(2), 136–143 (2021)

19. Pan, C., Ren, H., Wang, K., Xu, W., Elkashlan, M., Nallanathan, A., Hanzo, L.: Multicell MIMO communications relying on intelligent reflecting surfaces. IEEE Trans. Wireless Commun. 19(8), 5218–5233 (2020)
20. Wu, Q., Zhang, R.: Towards smart and reconfigurable environment: Intelligent reflecting surface aided wireless network. IEEE Commun. Mag. 58(1), 106–112 (2020)
21. Ning, B., Chen, Z., Chen, W., Fang, J.: Beamforming optimization for intelligent reflecting surface assisted MIMO: A sum-path-gain maximization approach. IEEE Wireless Commun. Lett. 9(7), 1105–1109 (2020)
22. Wang, P., Fang, J., Yuan, X., Chen, Z., Li, H.: Intelligent reflecting surface-assisted millimeter wave communications: Joint active and passive precoding design. IEEE Trans. Veh. Technol. 69(12), 14960–14973 (2020)
23. Guo, H., Liang, Y.-C., Chen, J., Larsson, E.G.: Weighted sum-rate maximization for reconfigurable intelligent surface aided wireless networks. IEEE Trans. Wireless Commun. 19(5), 3064–3076 (2020)
24. Zhang, Z., Dai, L.: A joint precoding framework for wideband reconfigurable intelligent surface-aided cell-free network. IEEE Trans. Signal Process. 69, 4085–4101 (2021)
25. Zhao, M.-M., Liu, A., Zhang, R.: Outage-constrained robust beamforming for intelligent reflecting surface aided wireless communication. IEEE Trans. Signal Process. 69, 1301–1316 (2021)
26. Liu, R., Li, M., Liu, Q., Swindlehurst, A.L.: Joint symbol-level precoding and reflecting designs for IRS-enhanced MU-MISO systems. IEEE Trans. Wireless Commun. 20(2), 798–811 (2021)
27. Zhang, S., Zhang, R.: Capacity characterization for intelligent reflecting surface aided MIMO communication. IEEE J. Sel. Areas Commun. 38(8), 1823–1838 (2020)
28. Kasai, H.: Fast optimization algorithm on complex oblique manifold for hybrid precoding in millimeter wave mimo systems. In: 2018 IEEE Global Conference on Signal and Information Processing (GlobalSIP), pp. 1266–1270. IEEE, Piscataway (2018)
29. Hong, S.H., Park, J., Kim, S.-J., Choi, J.: Hybrid beamforming for intelligent reflecting surface aided millimeter wave MIMO systems. IEEE Trans. Wireless Commun. 21(9), 7343–7357 (2022)
30. Wang, H., Fang, J., Li, H.: Joint beamforming and channel reconfiguration for RIS-assisted millimeter wave massive MIMO-OFDM systems. IEEE Trans. Veh. Technol. 72(6), 7627–7638 (2023)
31. Ning, B., Wang, P., Li, L., Chen, Z., Fang, J.: Multi-irs-aided multi-user mimo in mmwave/thz communications: A space-orthogonal scheme. IEEE Trans. Commun. 70(12), 8138–8152 (2022)
32. Singh, J., Srivastava, S., Jagannatham, A.K., Hanzo, L.: Joint transceiver and reconfigurable intelligent surface design for multiuser mmWave MIMO systems relying on non-diagonal phase shift matrices. IEEE Open J. Commun. Soc. 4, 2897–2912 (2023)
33. Zhang, X.-D.: Matrix Analysis and Applications. Cambridge University Press, Cambridge (2017)
34. Alhujaili, K., Monga, V., Rangaswamy, M.: Transmit mimo radar beampattern design via optimization on the complex circle manifold. IEEE Trans. Signal Process. 67(13), 3561–3575 (2019)
35. Ayach, O.E., Rajagopal, S., Abu-Surra, S., Pi, Z., Heath, R.W.: Spatially sparse precoding in millimeter wave MIMO systems. IEEE Trans. Wireless Commun. 13, 1499–1513 (2014)
36. Gautam, P.R., Zhang, L.: Hybrid precoding for millimeter wave MIMO: Trace optimization approach. IEEE Access 10, 66874–66885 (2022)
37. Vandenberghe, L., Boyd, S.: Semidefinite programming. SIAM Rev. 38(1), 49–95 (1996)
38. Luo, Z.-q., Ma, W.-k., So, A.M.-c., Ye, Y., Zhang, S.: Semidefinite relaxation of quadratic optimization problems. IEEE Signal Process Mag. 27(3), 20–34 (2010)
39. Liang, L., Xu, W., Dong, X.: Low-complexity hybrid precoding in massive multiuser MIMO systems. IEEE Wireless Commun. Lett. 3(6), 653–656 (2014)
40. Gautam, P.R., Zhang, L., Fan, P.: Hybrid MMSE precoding for millimeter wave MU-MISO via trace maximization. IEEE Trans. Wireless Commun. 23(3), 1999–2010 (2023)
41. Chiu, P.-N., Lin, Y.-P.: Statistical precoding for dual-polarized narrowband and wideband mmWave systems. In: 2021 15th International Conference on Signal Processing and Communication Systems (ICSPCS), pp. 1–6. IEEE, Piscataway (2021)
42. Lin, T., Cong, J., Zhu, Y., Zhang, J., Letaief, K.B.: Hybrid beamforming for millimeter wave systems using the MMSE criterion. IEEE Trans. Commun. 67(5), 3693–3708 (2019)
43. Bolcskei, H., Borgmann, M., Paulraj, A.: Impact of the propagation environment on the performance of space-frequency coded MIMO-OFDM. IEEE J. Sel. Areas Commun. 21(3), 427–439 (2003)
44. Yu, X., Shen, J., Zhang, J., Letaief, K.B.: Alternating minimization algorithms for hybrid precoding in millimeter wave MIMO systems. IEEE J. Sel. Top. Signal Process. 10, 485–500 (2016)
45. Lee, J., Lee, Y.H.: AF relaying for millimeter wave communication systems with hybrid rf/baseband mimo processing. In: 2014 IEEE International Conference on Communications (ICC), pp. 5838–5842. IEEE, Piscataway (2014)
46. Akdeniz, M.R., Liu, Y., Samimi, M.K., Sun, S., Rangan, S., Rappaport, T.S., Erkip, E.: Millimeter wave channel modeling and cellular capacity evaluation. IEEE J. Sel. Areas Commun. 32(6), 1164–1179 (2014)
47. Tse, D., Viswanath, P.: Fundamentals of Wireless Communication. Cambridge University Press, New York (2005)


**How to cite this article:** Gautam, P.R., Zhang, L., Fan, P.: MMSE-based passive beamforming for reconfigurable intelligent surface aided millimeter wave MIMO. IET Commun. 19, e12873 (2025). https://doi.org/10.1049/cmu2.12873